DLR-IB-FA-BS-2022-188

Optimization of filament wound cryogenic composite tanks with unconventional geometries for future aircraft configurations

Masterarbeit

Julius Biermann

Deutsches Zentrum für Luft- und Raumfahrt

MH-FA-56-FB03_v1.3

Institut für Faserverbundleichtbau und Adaptronik

DLR-IB-FA-BS-2022-188

Optimization of filament wound cryogenic composite tanks with unconventional geometries for future aircraft configurations

Zugänglichkeit:

Stufe 1 - Allgemein zugänglich: Der Interne Bericht wird elektronisch ohne Einschränkungen in ELIB abgelegt. Falls vorhanden, ist je ein gedrucktes Exemplar an die zuständige Standortbibliothek und an das zentrale Archiv abzugeben.

Braunschweig, *Oktober, 2022*

Der Bericht umfasst: 57 Seiten

Abteilungsleiter:
Dr. Tobias Wille

Autor:
Julius Biermann

Autor 2 / Betreuer:
Sebastian Freund

Deutsches Zentrum für Luft- und Raumfahrt

Deutsches Zentrum
für Luft- und Raumfahrt
German Aerospace Center

Institut Supérieur de l'Aéronautique et de l'Espace
and German Aerospace Center

MASTER THESIS

Optimization of filament wound cryogenic composite tanks with unconventional geometries for future aircraft configurations

Author:
Julius BIERMANN

Supervisors:
Dr.-Ing. Sebastian FREUND
Prof. Frédéric LACHAUD

A thesis submitted in fulfillment of the requirements
for the degree of Master of Science

in

Aerospace Engineering
Aerospace Structures | Aircraft Design and Operations

October, 2022

Declaration of Authorship

This assignment is entirely my own work. Quotations from secondary literature are indicated by the use of inverted commas around ALL such quotations AND by reference in the text or notes to the author concerned. ALL primary and secondary literature used in this piece of work is indicated in the bibliography placed at the end, and dependence upon ANY source used is indicated at the appropriate point in the text. I confirm that no sources have been used other than those stated.

I understand what is meant by plagiarism and that plagiarism is a serious examinations offence that may result in disciplinary action being taken.

Signed: _____

Date: _____

Abstract

A promising technology for minimizing CO_2 emissions in aviation is the use of liquid hydrogen stored under cryogenic conditions. However, at the same time, it presents challenges with regard to the integration of the tank in the aircraft due to its low volumetric energy density. One concept pursues the integration in the rear conical fuselage section, which requires a high flexibility of the tank geometry in combination with a low mass. From this derives the objective of the work to extend an existing software for the simulation of the winding process for cylindrical tanks by conical geometries as well as different dome types in order to analyze and evaluate different tank configurations also with respect to the impact on the overall aircraft design. Based on a relative geometric parametrization defined by the ratios of the radial and longitudinal dimensions of the tank, the simulation software was extended and torispherical and isotensoid dome contours were implemented in addition to hemispherical and elliptical ones with variable semi-axis ratios. In a preliminary analysis, the described dome types for cylindrical and conical tank shapes were compared and the resulting masses as well as geometric dimensions were evaluated. Regardless of the tank shape, isotensoid domes offer the best compromise of the criteria considered. Based on these findings and the previously implemented geometric enhancements to the software, the effects of different tank shapes were investigated based on an existing aircraft concept. For this purpose, the position of the tanks in the predefined design space was varied in such a way that cylindrical as well as purely conical tank shapes were created, evaluated and the influence on the aircraft mass was assessed. It could be concluded that conical tank shapes, despite the higher mass, have advantages over cylindrical shapes due to the shorter fuselage length. These findings were confirmed in the surrogate model, in which the influence of the various geometric design parameters on the tank mass and surface area were analyzed.

Eine vielversprechende Technologie zur Minimierung von CO_2 Emissionen in der Luftfahrt ist der Einsatz flüssigen und unter kryogenen Bedingungen gespeicherten Wasserstoffs. Dieser weist allerdings zeitgleich aufgrund der geringen volumetrischen Energiedichte Herausforderungen in Bezug auf die Integration des Tanks im Flugzeug auf. Ein Konzept verfolgt die Integration in der hinteren konischen Rumpfsektion, was eine hohe Flexibilität der Tankgeometrie in Verbindung mit einer geringen Masse voraussetzt. Daraus leitet sich die Zielsetzung der Arbeit ab, eine bestehende Software zur Simulation des Wickelprozesses für zylindrische Tanks um konische Geometrien sowie verschiedene Domtypen zu erweitern und diese, auch im Kontext des Flugzeugdesigns, zu analysieren und zu bewerten. Basierend auf einer relativen geometrischen Parametrisierung, die die radialen und longitudinalen Dimensionen des Tanks ins Verhältnis setzt, wurde die Simulationssoftware erweitert, sowie neben halbkugelförmigen und elliptischen Domkonturen mit variablen Halbachsenverhältnissen auch torispherische und isotensoide Domformen implementiert. In einer Voranalyse wurden die beschriebenen Domtypen für zylindrische und konische Tankformen gegenübergestellt und die resultierenden Massen sowie geometrischen Dimensionen bewertet. Unabhängig von der Form des Tanks bieten isotensoide Döme den besten Kompromiss der in Betracht gezogenen Kriterien. Basierend auf diesen Erkenntnissen und den zuvor implementierten geometrischen Erweiterungen der Software wurden auf Basis eines bestehenden Flugzeugkonzepts die Auswirkungen verschiedener Tankformen untersucht. Dazu wurde die Position der Tanks im vordefinierten Designraum so variiert, dass zylindrische als auch rein konische Tankformen erstellt, ausgewertet sowie der Einfluss auf die Flugzeugmasse bewertet wurden. Daraus konnte geschlussfolgert werden, dass konische Tankformen, trotz der höheren Eigenmasse, aufgrund der geringeren Rumpflänge, Vorteile gegenüber zylindrischen Formen haben. Diese Erkenntnisse konnten im Ersatzmodell bestätigt werden, in dem der Einfluss der verschiedenen geometrischen Designparameter auf die Tankmasse sowie -oberfläche analysiert wurden.

Acknowledgements

The preparation of my master thesis required the help, support and willingness of various people, whom I would like to thank in the context of this acknowledgement.

A big thank you goes to my supervisor, Dr.-Ing. Sebastian Freund, who was always patient and helpful, answered my questions with great dedication and gave me the right hints and directions.

Furthermore, I would like to thank Dr.-Ing. Tobias Wille and his team, who welcomed me very openly and gave me the opportunity to write my thesis.

In addition, I would like to thank Prof. Frédéric Lachaud, who supervised my master's thesis from the university side.

Finally, I would like to express my sincere gratitude to my family, who made it possible for me to pursue my desire to study abroad and, despite the distance and any problems and doubts related to the pandemic, always supported me, helped me and gave me good advice.

Contents

List of Figures

List of Tables

List of Abbreviations

CAGR	Compound Annual Growth Rate
CG	Center of Gravity
CO_2	Carbon dioxide
LH_2	Liquid Hydrogen
OAD	Overall Aircraft Design
RPK	Revenue Passenger Kilometers

List of Symbols

α	winding angle	$(^\circ)$
α	Geometric parameter	
β	Geometric parameter	
γ	Geometric parameter	
δ	Geometric parameter	
κ_g	principal curvature vector tangential to surface	
κ_n	principal curvature vector normal to surface	
λ	slippage coefficient	
N_m	mandrel rotational speed	$(\mathrm{rad\,s^{-1}})$
v_c	carrier linear speed	$(\mathrm{m\,s^{-1}})$

Chapter 1

Introduction

1.1 Motivation

The climatic conditions have developed drastically since the 19^{th} century due to human activities in the context of industrialization. According to the National Oceanic and Atmospheric Administration, the earth's temperature has risen by an average of 0.08 °C per decade since 1880, and by as much as 0.18 °C per decade in the period from 1981 to the present [1].

The main contribution to this is made by CO_2 emissions, which can be divided into various origin sectors. With 7.2 Gt CO_2, corresponding to a share of 23 %, the transport sector was a decisive contributor to global energy-related CO_2 emissions in 2020. Of this, approximately 10 % is attributable to aviation [2, 3]. In addition, there are other factors that have a considerable influence on climatic change. Nearly 80 % of these influences are due to nitrogen oxides and contrails [4].

To counteract these developments and reduce the greenhouse gas emissions, the Paris Agreement was established in 2015, setting the goal of "[h]olding the increase in the global average temperature to well below 2 °C above pre-industrial levels and pursuing efforts to limit the temperature increase to 1.5 °C above pre-industrial levels" [5].

In parallel with the CO_2 reduction targets set, passenger numbers have shown steady growth in recent years. Despite the brief strong decline in passenger numbers due to the Corona pandemic, the Airbus Global Market Forecast predicts a Compound Annual Growth Rate (CAGR) of 3.9 % in Revenue Passenger Kilometers (RPK) from 2019 to 2040 [6].

In order to reconcile these opposing developments, a radical shift from fossil fuels to sustainable and broadly scalable concepts is required. The use of hydrogen as an energy carrier represents a promising technology, especially for civil aviation. Particularly in its liquid state (LH_2) at -253 °C, hydrogen exhibits advantages compared to highly compressed gaseous hydrogen due to the higher structural tank mass. Extended to fossil fuels, these include the following:

- The energy per unit mass (141.8 MJ/kg) is with a factor of 3.3 significantly higher than conventional fuels, leading to a decrease of the required fuel mass [7].
- The combustion of hydrogen produces only water in vaporised state as a byproduct. In terms of local air quality, up to 90 % less nitrogen oxides are generated during combustion compared to kerosene fuel and the formation of particulate matter is eliminated [8].

However, the use of hydrogen, especially in its liquid form, poses profound technological challenges, particularly with regard to its storage, which in turn has an impact on different factors of the aircraft design. These include the following:

- The storage in liquid form requires an efficient insulation system aiming to reduce the boil-off rate and maintaining the internal tank pressure below a defined threshold. If this limit is exceeded, gaseous hydrogen must be discharged, leading to fuel loss and thus to degraded performance [7].
- The ratio of the volumetric energy density of kerosene and liquid hydrogen is approximately four, corresponding to a four time higher storage volume. This reduces the space available for payload and can in addition affect the aerodynamic efficiency [9].
- Due to the higher storage volume of hydrogen and the space requirement of the related subsystems, the fuel tanks cannot be integrated in the wings as in previous aircraft configurations [7].
  As a result, the tanks must be installed along the aircraft's longitudinal axis, which in turn has a considerable influence on the stability of the aircraft due to the leverage effect for an increasing distance from the center of gravity (CG) [9].

To address both the stability challenges around the aircraft's pitch axis and the high storage volume of hydrogen, lightweight and geometrically flexible tank shapes are needed to achieve high volumetric efficiency by matching the fuselage architecture.

1.2 Objective of the work

Based on this, the scientific question is derived, what influence the tank shape has on the properties and characteristics on the tank as well as on the global aircraft design, especially in relation to the mass.

The conical tank shape, which is based on the architecture of the aircraft fuselage, is to be determined by a dimensionless geometric parameterization allowing to design different tank geometries in the preliminary design state.

Based on this, the layer structure determined by an optimizer is to be simulated with winding software giving detailed information about the final tank design including specific data such as mass and geometrical properties.

Building upon this, an evaluation is performed which is based on various local and global evaluation criteria and which has as the objective to compare different tank configurations in order to derive an optimized positioning of the tank in a given aircraft environment.

In the final step is to develop a surrogate model is created that allows a basic assessment of the simulation results in the defined parameter space based on a regression method. Because application-specific simulations are not required, this model can be used in the preliminary design of the complete aircraft.

Chapter 2

Literature review

2.1 Filament winding

Filament winding is a manufacturing process in which a continuous fiber band is uniformly and regularly placed on a mandrel. To ensure complete coverage of the body and to realize an application-specified fiber orientation, either the mandrel or the application head is rotated and moved in axial direction [10, 11].

The manufacturing possibilities are limited to geometries that do not have high concave curvatures due to the occurrence of fiber bridging effects. As the number of degrees of freedom increases, this process can also be used to produce non-rotationally symmetrical bodies. Examples are tubes, gas or liquid storage tanks but also more complex bodies like T-joints can be produced with this process [12].

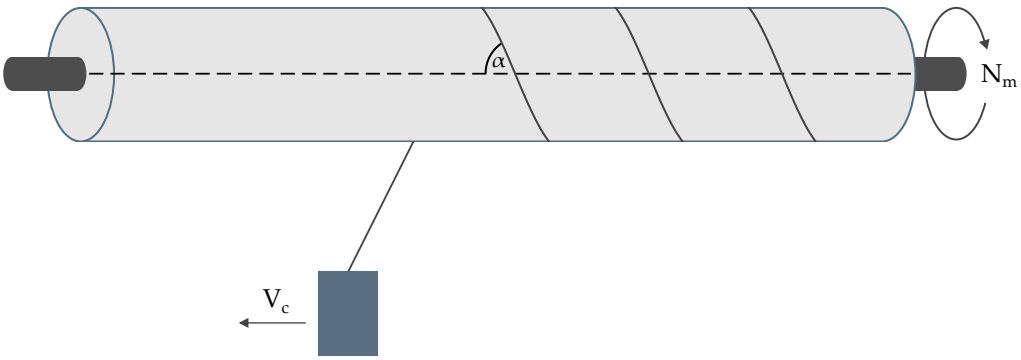

Fig. 2.1. Schematic illustration of the filament winding principle

Basically, this manufacturing technique is distinguished between two different methods, wet and prepreg winding. In the wet winding process, the dry fibers are passed through a resin bath before being placed on the mandrel. This technique is cost-effective, but has disadvantages in terms achieving a constant resin content due to the dependence on various interrelated factors, which in turn has a negative impact on the reproducibility [13].

In the prepreg process, pre-impregnated fibers are wound onto the mandrel without an intermediate step. As a result of the more constant manufacturing parameters, such as the resin content, a higher quality can be reached with a better reproducibility compared to the wet process technology. However, this process has disadvantages in terms of cost and manufacturing due to more complex subsequent production steps [13].

One of the main design parameters is the winding angle α, which indicates the orientation of the fiber with respect to the longitudinal axis of the body (Figure 2.1).

In addition to the geometry of the winding body, this quantity is also dependent on the axial and rotational speed of the laying head and mandrel respectively and can be determined for a rotational body with a constant cross section using the following equation.

$$tan(\alpha) = \frac{2 \cdot \pi \cdot R \cdot N_m}{60 \cdot v_c} \tag{2.1}$$

With R being the mandrel radius, N_m being the mandrel rotational speed and v_c being the carrier linear speed [14].

2.1.1 Mandrel and liner

The mandrel serves as a shaping manufacturing base on which the fibers are wound in the manufacturing process. This results in various requirements that must be considered in the design of the mandrel, which include the following

- The mandrel must have a sufficiently high inherent stiffness to withstand the occurring compression loads imposed by the winding force.
- The detachment of the laminate from the mandrel surface must be ensured. This is done with the help of release agents that are applied to the mandrel.
- The mandrel must be removable after completion of the manufacturing process [15].

Although structural safety is still assured, matrix cracking can cause leakage even in low-pressure and liquid tanks, requiring an additional liner. These usually consist of thin metal or polymer layers applied inside the tank [16]. If the liner is sufficiently rigid, it can also perform the function of mandrel, which has advantages in terms of the above requirements especially due to the fact that the mandrel must not be removed after the manufacturing process [12].

2.2 Fiber trajectories

In filament winding, the trajectory of the fiber with the corresponding orientation cannot be set arbitrarily due to the fiber stability requirements. To ensure process reliability, slipping of the fiber on the mandrel and its separation must be avoided [17]. In order to meet these requirements, two different trajectory types are distinguished, geodesic and non-geodesic trajectories.

2.2.1 Geodesic fiber trajectories

In a theoretically considered frictionless system, the path of the fiber is unique for a given starting point and orientation. This path is defined by the minimum curve length between any two points on a three-dimensional surface and is called geodesic path. In this condition, the fiber does not show any slippage on the mandrel under axial load forces and can thus be considered stable [17, 18].

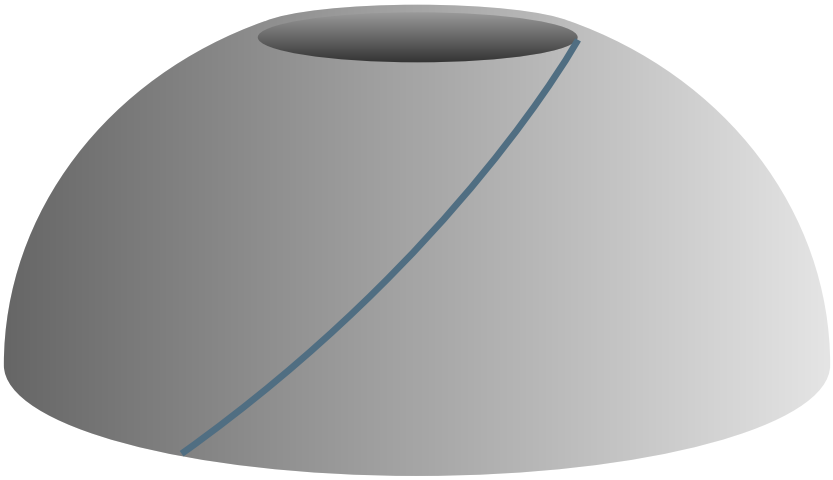

Fig. 2.2. Geodesic trajectory on a shell of revolution

The uniqueness of the fiber path solution reduces the computational cost, but severely limits the design options of the winding patterns as well as the geometry of the mandrel [19].

2.2.2 Non-geodesic fiber trajectories

To widen the design freedom and better match the orientation of the layers to the required mechanical properties of the structure, non-geodesic paths can be used [20].

In contrast to geodesic paths, these trajectories take into account the friction between the fiber and the substrate, which allow to counteract forces acting axially to the fiber direction and thus to realize stable fiber paths unequal to the minimum curve length [19].

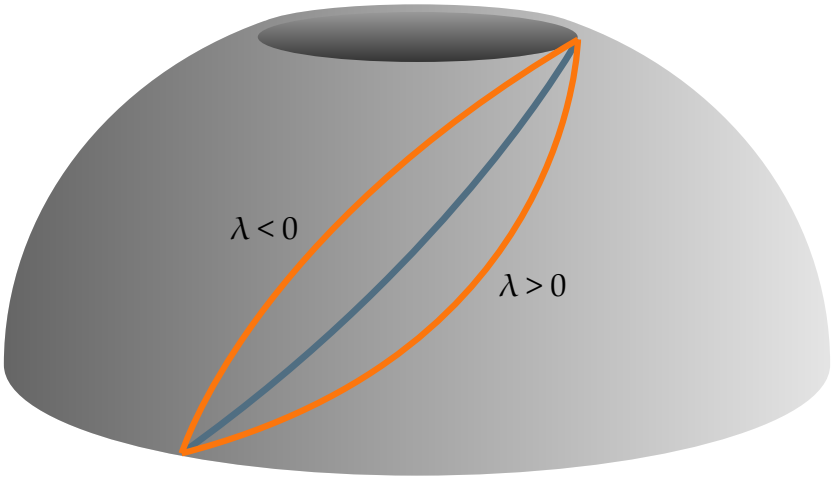

Fig. 2.3. Non-geodesic trajectory on a shell of revolution

To ensure the stable condition of the fiber on the surface, the non-slippage criterion must be met. This provides information on the slippage tendency between the fiber and the surface and is used to determine the possible winding patterns [12].

Considering the balance of forces in axial and longitudinal fiber direction and the condition that the friction force is below the maximum static friction, the mathematical expression of the slippage coefficient can be derived, which is the following

$$\lambda = \frac{\kappa_g}{\kappa_n} \tag{2.2}$$

with κ_n being the component of the principal curvature vector normal to the surface at a point (normal curvature) and κ_g being the component of the curvature vector tangential to the surface (geodesic curvature).

Using this expression and considering the coefficient of maximum static friction μ_{max} between the mandrel or the previous layer respectively, the equation for the non-slippage criterion can be determined [20].

$$|\lambda| \leq \mu_{max} \tag{2.3}$$

The effects of a slippage coefficient unequal to zero on the fiber path are shown qualitatively in Figure 2.3.

2.2.3 Mathematical representation of fiber trajectories

The winding angle of geodesic and non-geodesic paths can be determined by a mathematical expression. The starting point for the derivation of this equation is the vector parameterization of a generic surface of revolution in polar coordinates, which is defined as follows and graphically illustrated in Figure 2.4 [12].

$$S(u,v) = \{f(u)cos(v), f(u)sin(v), g(u)\} \quad (f(u) \leq 0) \tag{2.4}$$

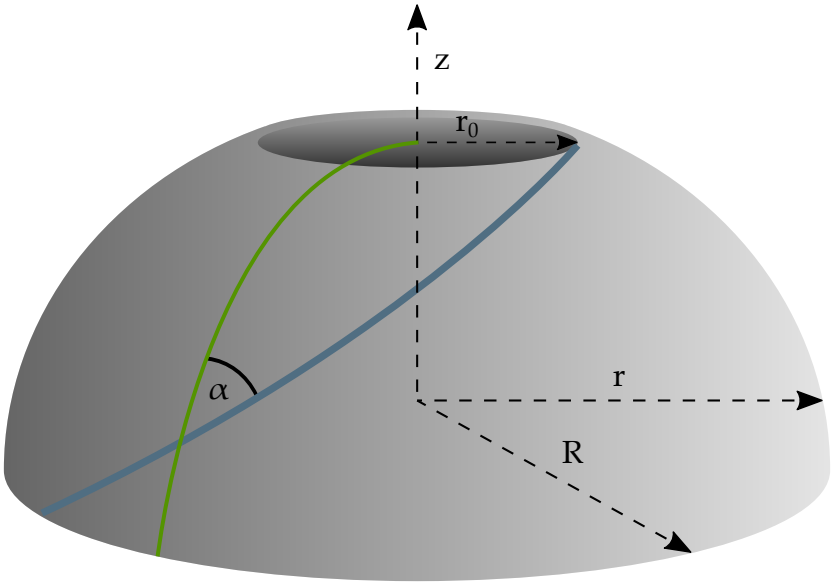

Fig. 2.4. Shell of revolution

Using the mathematical expression of the normal curvature κ_n and the geodesic curvature κ_g, the differential equation for the determination of non-geodesic trajectories with respect to α and z can be obtained with various intermediate operations [12].

$$\frac{d\alpha}{dz} = \lambda \left[\frac{sin(\alpha)tan(\alpha)}{r} - \frac{r''}{1+r'^2} cos(\alpha) \right] - \frac{r'tan(\alpha)}{r} \tag{2.5}$$

The solution of the differential equation for $\lambda = 0$ corresponds to the Clairaut equation, which can be used to determine the geodesic trajectories on a surface of revolution [19].

$$\alpha = arcsin\left(\frac{r_0}{r}\right) \tag{2.6}$$

The variation of the local winding angle as a function of the radius coordinate for a body with a r_0 to R ratio of 0.3 is shown in Figure 2.5.

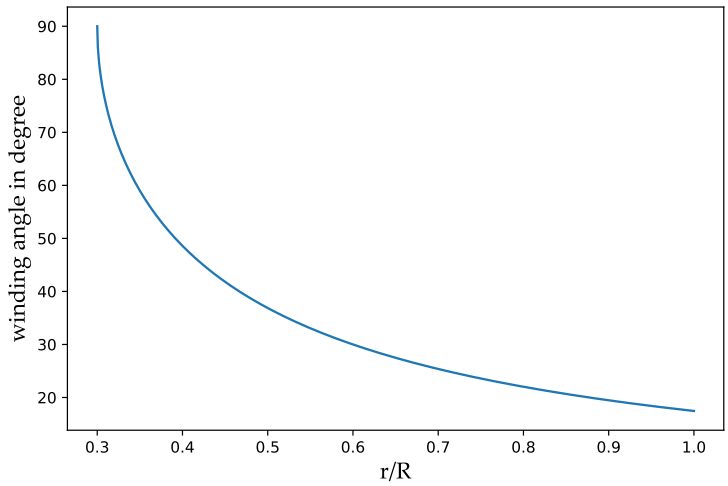

Fig. 2.5. Local winding angle depending on r/R

2.3 Geodesic winding patterns

Depending on the winding angle, geodesic winding patterns can be divided into three groups, planar or polar, helical and hoop winding [21].

Polar windings are layers with a low winding angle, according to the definition smaller than 5°. The minimum feasible angle is determined by the polar opening radius and the length of the winding body and each completed pattern corresponds to a single reinforced layer [19].

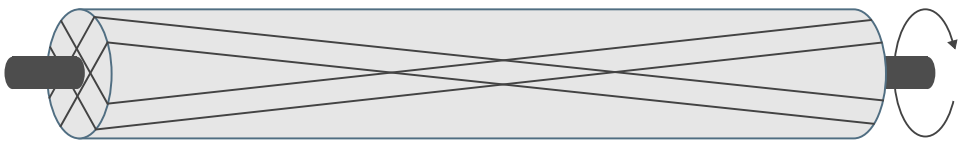

Fig. 2.6. Polar winding

Helical windings are characterized by an fiber orientation between 5° and 80° with respect to the longitudinal axis of the body. These windings are wound alternately in positive and negative orientations, resulting in a pattern with double the number of layers [12].

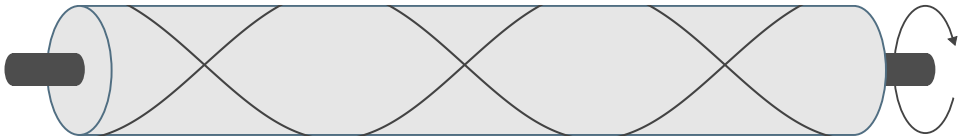

Fig. 2.7. Helical winding

Hoop windings can be considered as a special form of helical windings with an orientation angle close to 90° leading to a single layer of reinforcement.

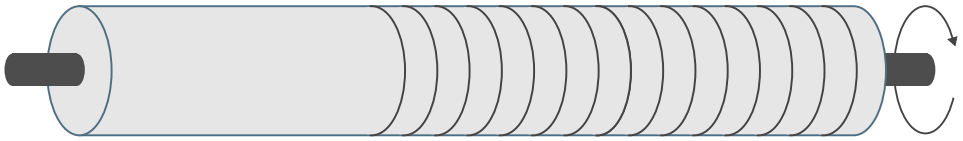

Fig. 2.8. Hoop winding

The maximum feasible angle for a rotational body with a constant cross section is defined by the diameter and width of the deposited fiber bundle and can be obtained using the following expression.

$$\alpha_{max} = 90° - arctan\left(\frac{w_{tow}}{2\pi R}\right) \tag{2.7}$$

The transition from helical to hoop windings can be achieved by manually cutting and reattaching the fiber bundle on the mandrel with the defined orientation. Alternatively, the fiber orientation can be changed gradually by using non-geodesic trajectories, which optimizes the continuity of the manufacturing process, but requires transition layers and thus represents a deviation from the structurally ideal layer structure [22].

2.4 Tank geometry

The tank geometry represents a compromise of various factors that are highly dependent on the application. In addition to thermal properties and load cases, resulting among others from the pressurization of the tank and the inertial forces due to the tare weight and the mass of the stored medium, these include above all geometric restrictions given by the tank environment.

Widely used for storage of cryogenic liquids are spherical or cylindrical tank shapes. Due to the minimal surface-to-volume ratio of spheres, the passive heat flux into the tank is low which in turn results in a reduction of the boil-off rate. However, the volumetric efficiency is lower compared to cylindrical geometries as a consequence of the cylindrical or conical fuselage structure. With a higher surface-to-volume ratio and a higher volumetric efficiency related to cylindrical fuselage shapes, cylindrical tanks exhibit opposite properties [23].

The end caps, called domes, of cylindrical and conical tanks can have different contours mainly depending on the material and loading as well as manufacturing aspects. The most commonly used dome types are considered in this work defined in more detail below.

2.4.1 Hemispherical domes

Hemispherical domes are the simplest dome shape from a geometric point of view. They are fully defined by two geometrical parameters, the polar opening radius and the radius R, which, for a cylindrical body, corresponds to the cylindrical radius and taking into account the tangent continuity at the transition from the dome to the tank body. The polar opening radius has no dependence on other geometrical parameters and can therefore be chosen in compliance with the manufacturing and design-related constraints.

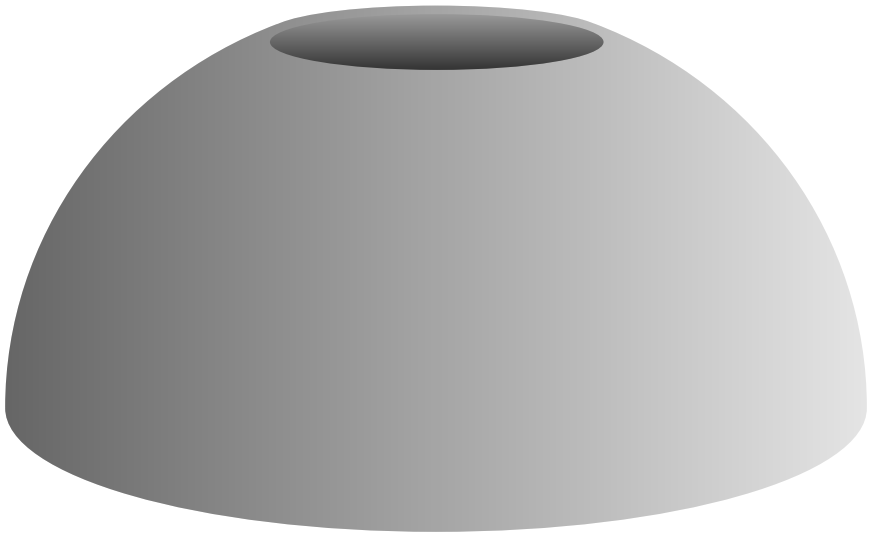

Fig. 2.9. Hemispherical dome

For an isotropic material, hemispherical domes represents the ideal structural shape for pressurized vessels [12]. However, for a constant tank length, hemispheres have disadvantages compared to other dome geometries in terms of volumetric efficiency.

2.4.2 Elliptical domes

In addition to the polar opening radius, an elliptical dome is defined by two other quantities, the minor and major semi-axes. The characterization of the cross-sectional area can be done by the ratio of their respective semi-axes, given by the following equation.

$$\epsilon = \frac{b}{a} \tag{2.8}$$

The major semi-axis (a) is perpendicular to the longitudinal axis and corresponds the cylindrical diameter in a cylindrical tank while the minor axis (b) is parallel to the longitudinal axis and can be determined by specifying the ratio of both semi-axes respecting the constraint given above.

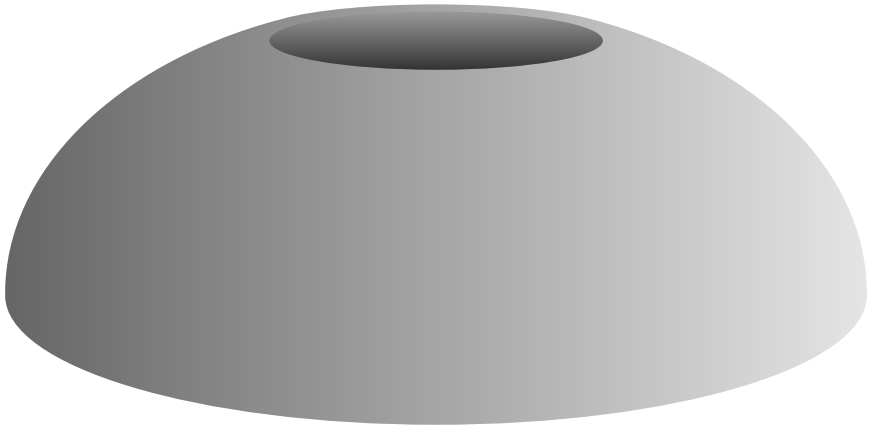

Fig. 2.10. Elliptical dome

Compared to hemispherical domes, elliptical flows have a higher flexibility due to the higher number of selectable geometrical parameters and can thus be adapted to the given constraints.

2.4.3 Isotensoid domes

As an alternative to changing the ply structure and thereby achieving the optimum weight, the dome geometry can be adapted to the prevailing load case in order to improve the structural performance. Obtaining the optimal solution in terms of weight implies that all fibres are submitted to a uniform tensile loading along their length giving an geodesic-isotensoid dome contour which is defined by the maximum radius and the polar opening radius [24].

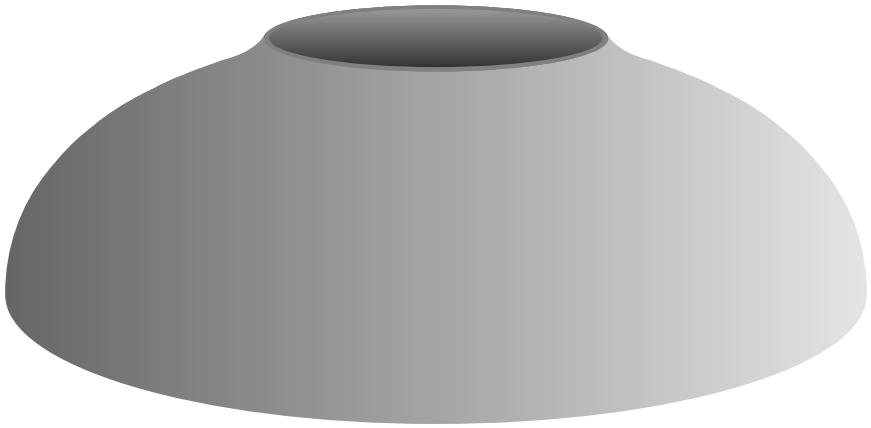

Fig. 2.11. Isotensoid dome

Depending on these two parameters, the contour can be determined mathematically using a discrete point cloud according to the patent specification [25]. Starting from the initial conditions

$$r = R \quad ; \quad z = 0 \tag{2.9}$$

referring to Figure 2.4, the Clairaut equation 2.6 is used to determine the local winding angle alpha.

The forces in meridian and hoop direction on a single dome element located at an angle ψ, which is defined as the angle between meridian at a given position r and the meridian at the initial r condition, and their ratio are expressed by

$$N_m = \frac{r}{cos\psi} R \tag{2.10}$$

$$N_h = \frac{r}{cos\psi} \left(2R - \frac{N_m}{r_c} \right) \tag{2.11}$$

$$\frac{N_h}{N_m} = tan^2\alpha \tag{2.12}$$

Combining these equations and solving for r gives the expression for the determination of the radius of curvature r_c is obtained

$$r_c = \frac{r}{cos\psi(2 - tan^2\alpha)} \tag{2.13}$$

By incrementing the angle ψ starting from $\psi = 0$, the r and z coordinates can be obtained with the following relationships

$$r = R - \sum r_c \cdot \Delta\psi \cdot sin\psi \tag{2.14}$$

$$z = \sum r_c \cdot \Delta\psi \cdot cos\psi \tag{2.15}$$

Due to the mathematical indefiniteness of equation 2.13 for a winding angle of $\alpha \geq 54.7°$, the contour can only be determined with these mathematical relationships in a radius interval from R to $1.22r_0$.

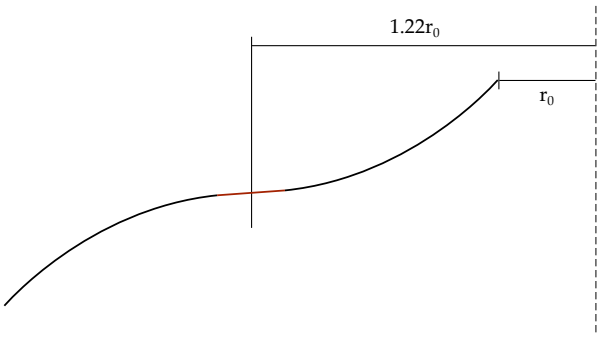

Fig. 2.12. Contour definition

The dome contour in the non-defined area can be determined starting from the polar opening via the same mathematical relationships, with the difference that the curvature is reversed and the angle ψ is decremented. Since the curvature of both subsegments approximate a straight line, these two contours are connected with a straight line and as a whole give the contour of the isotensoid dome as depicted in Figure 2.12 [25].

2.4.4 Torispherical domes

Another dome shape is the torispherical head which contour is, in contrast to the hemispherical dome, characterized by a central radius of and two adjacent corner radii, the curvature of which is standardized according to DIN 28011.

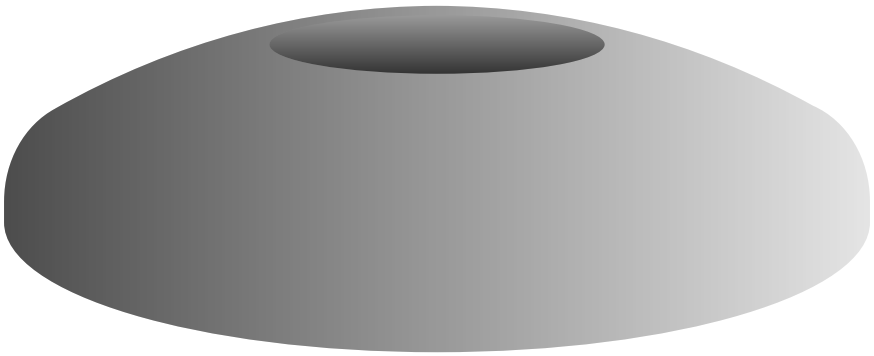

Fig. 2.13. Torispherical dome

Despite the different radii of curvature, the contour of the dome is completely defined by the specification of the cylindrical diameter and the polar opening radius and by taking into account the tangent continuity at the transition points of the radii and the cylindrical tank segment with the following expressions.

$$r_1 = d_{cyl} \tag{2.16}$$

$$r_2 = 0.1 \cdot d_{cyl} \tag{2.17}$$

The resulting contour line, taking into account the geometric parameters and mathematical constraints explained, can be seen in the figure below.

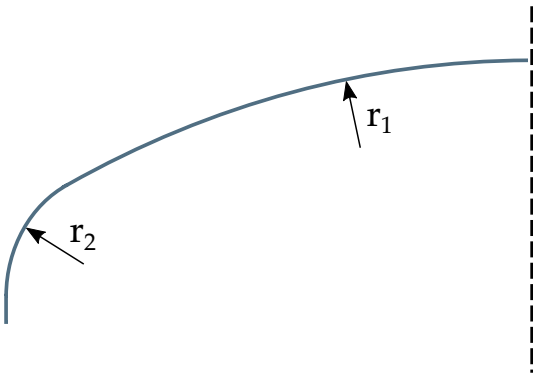

Fig. 2.14. Radii for torispherical dome

Chapter 3

Methodology for conical tank design

3.1 Parameterization of the tank geometry

In the preliminary stage of the development process, a relative parameterization is used to geometrically define the tank shape. This sets the different axial and radial lengths in relation to each other and thus enables a flexible geometrical design within a constrained design space without the specification of absolute values.

A generalized tank shape with the definitions of the respective geometric quantities is shown in Figure 3.1, consisting of a cylindrical and conical section with a transition radius as well as two dome heads at both extremities of the tank.

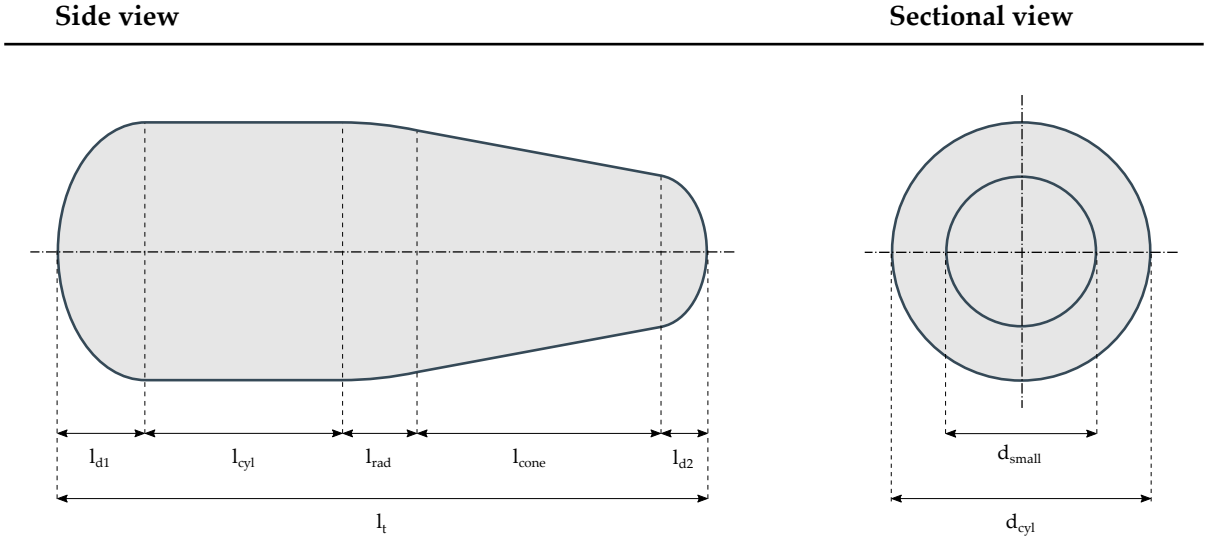

Fig. 3.1. Geometrical definitions of the tank

In the OAD environment, the cylindrical tank diameter and volume are usually specified as absolute values since these quantities are dictated by the architecture of the fuselage and the amount of fuel required for the flight mission. Considering these constraints and the geometrical definitions given above, the following parameters are derived

$$\alpha = \frac{d_{cyl} - d_{small}}{d_{cyl}} \tag{3.1}$$

Parameter α relates the normalized difference of the cylindrical diameter d_{cyl} and the small diameter of the conical section d_{small} and describes the conicity in radial direction of the tank for a constant radius length l_{rad} and conical length l_{cone}.

$$\beta = \frac{l_{rad} + l_{cone}}{d_{cyl}} \tag{3.2}$$

Parameter β is defined as the ratio of the total length of the conical segment consisting of the the length of the radius section l_{rad} and the conical section l_{cone} and the cylindrical diameter d_{cyl}. Contrary to parameter α, β depicts the conicity in axial direction assuming a constant diameter d_{small}.

$$\gamma = \frac{l_{rad}}{l_{rad} + l_{cone}} \tag{3.3}$$

Parameter γ gives the normalized proportion of the radius length l_{rad} to the total length of the conical section l_{rad} and l_{cone}. By adjusting this value, the distribution of the radius and conical section can be varied along the axial direction.

$$\delta = \frac{l_{dome}}{0.5 \cdot d_{dome}} \tag{3.4}$$

Parameter δ indicates the ratio of the two semi-axes of the respective domes. For the dome connected to the cylindrical part of the tank, the semi-axes correspond to the sizes l_{d1} and $d_{cyl}/2$. Due to the required tangent continuity at the transition from the conical segment to the adjoining dome, the semi-axes are dependent on the conicity and cannot be determined with the geometric quantities given in Figure 3.1.

Moreover, this parameter only represents ellipsoidal and hemispherical domes (ratio of the two semi-axes equals 1) and does not provide any significance for the geometrical properties of isotensoid and torispherical domes, which is why this parameter is not considered for these dome types. The cylindrical tank length, which must meet a software-specific minimum value of 150 mm due to the referencing of the simulation software used in the following design step, is determined by the volume difference of the defined tank volume and the partial volumes of the conical part and the tank domes.

In case the cylindrical length is below the presupposed minimum dimension of the simulation software, the axial and radial sizes are scaled down by the same factor, so that the parameters remain constant but the individual geometric sizes are adjusted to the volume requirement. This has the effect of reducing the previously defined cylindrical diameter. However, this methodology has the advantage that the conicity of the conical tank segment is kept constant, which simplifies implementation in a given aircraft fuselage architecture.

The influence of the various parameters on the tank contour can be seen in the Figure 3.2. The tank configurations shown have a constant volume and cylindrical diameter and the default parameters of $\alpha = 0.5$, $\beta = 1.5$, $\gamma = 0.5$ and both $\delta = 0.5$.

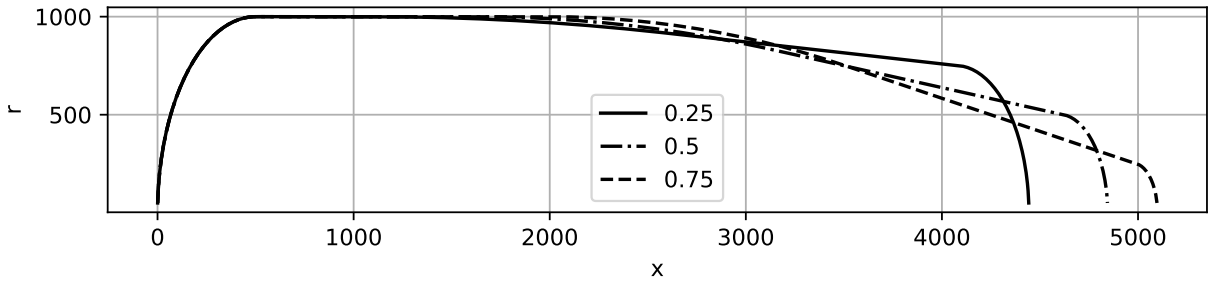

(a) Variation of parameter α

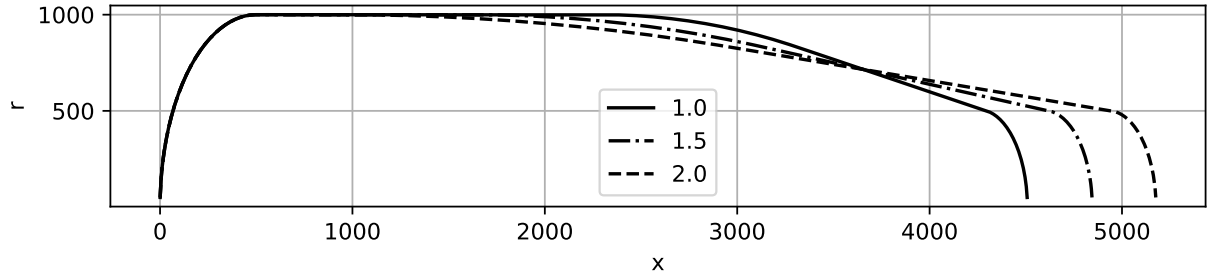

(b) Variation of parameter β

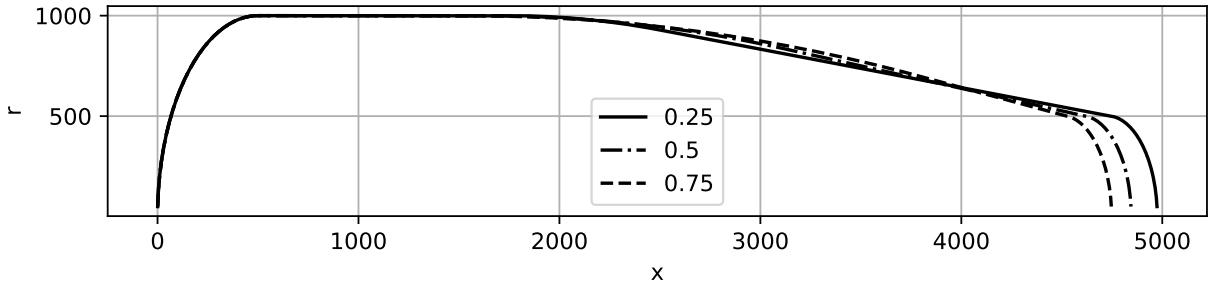

(c) Variation of parameter γ

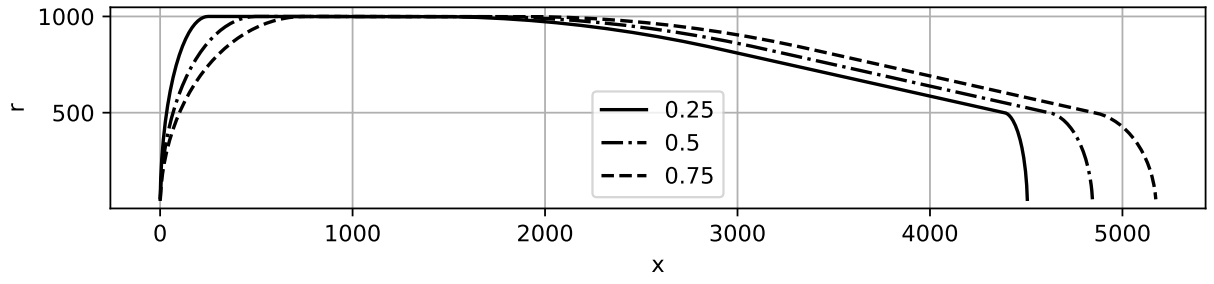

(d) Variation of parameter δ

Fig. 3.2. Variation of the geometrical parameters

3.2 Simulation

In the following step, the design of the layer structure is established on the basis of the previously determined geometry of the tank. The functions required for the design of the layup are provided by the software *µDesigner* from *Mefex*, among others. The simulation of the manufacturing process integrated in the design strategy is carried out by the winding software *µWind*. The winding angles determined in the iterative process are implemented in the simulation software and thus enable a progress-dependent determination of various parameters.

3.2.1 Pre-processing

The design has a dependency on various factors, which include the following:

- **Design:** Under the design aspects, all factors belonging to the tank design in the broadest sense are considered. These are the structural safety factor, the internal tank pressure, which in turn include the operating pressure, the minimum pressure and the burst pressure. Furthermore, the hydrostatic pressure and the resulting requirements according to CS 25.963 (d) can be taken into account depending on the position of the tank in the aircraft. In addition, based on the *Puck* failure criterion, the tank can be designed for either fiber or inter fiber failure.
- **Geometry:** The contour of the liner as well as the polar opening radius gives the minimum feasible orientation angle between the meridian and the fiber measured on the cylindrical tank segment, which is obtained with a function provided by the design software.
- **Manufacturing:** Further limitations are given by the manufacturing capabilities. These include the maximum deposit angle that can be realized by the winding machine, neglecting the hoop layers.
- **Material:** Additionally, the material characteristics are incorporated into the design of the layer structure. These include mechanical properties, such as the fiber volume fraction and Young's modulus as well as fiber and resin type in order to fully define the material behavior. Besides the material characteristics, the properties of the composite are specified. These include the roving parameter such as the thickness and width of the layer as well as the specific density and tex number.

3.2.2 Processing

Applying the design arguments, the optimized layer structure is derived using an iterative process with the optimization target to minimize the material failure according to the *Puck* criteria. The iterative calculations are performed by a developed Python code and partial functions of the software *µDesigner* using a Python interface. The schematic flow of the program is shown in Figure 3.3.

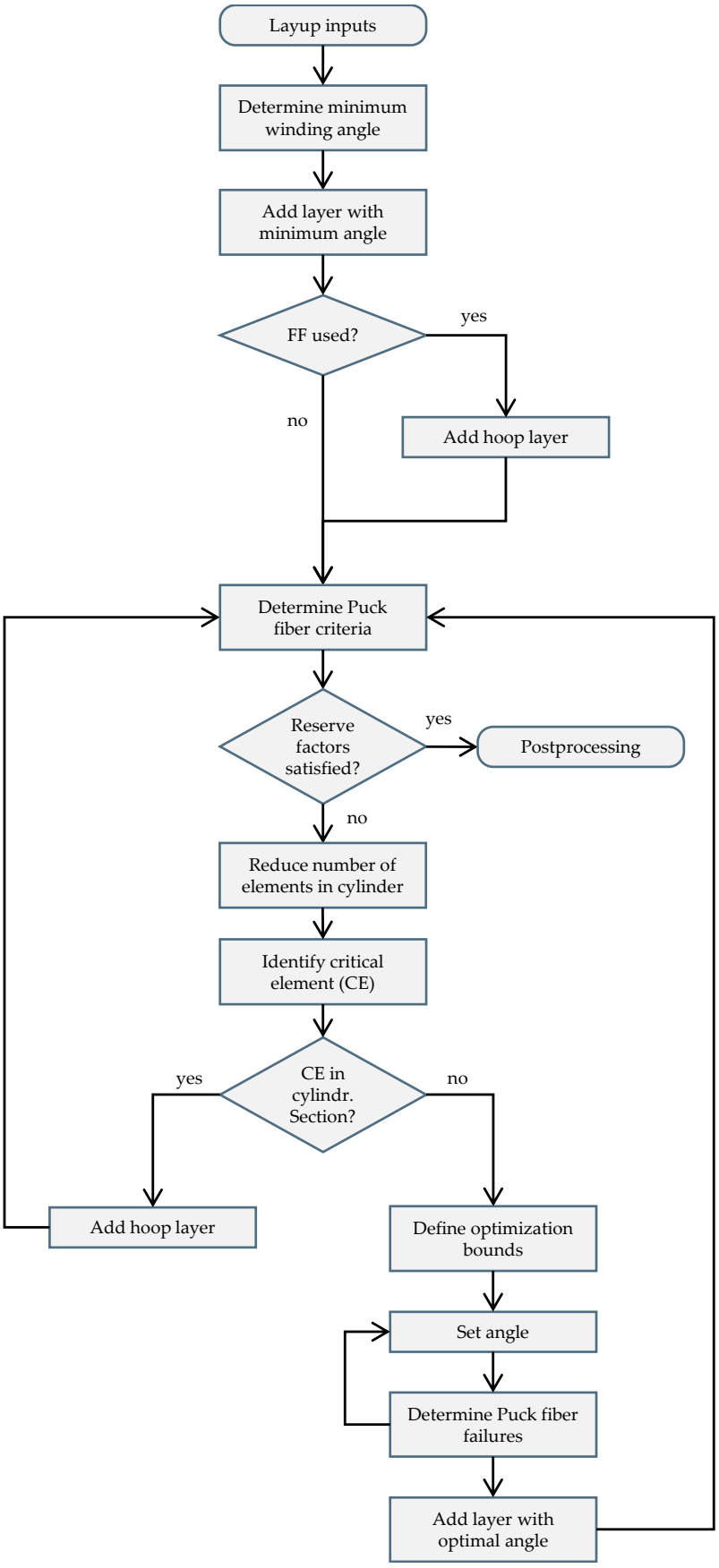

Fig. 3.3. Program flow optimizer

In the first step, the minimum winding angle is determined as a function of the geometry and the pole opening radius of the tank and, depending on this, the first layer is winded with the obtained orientation. Depending on the failure criterion set in the design settings, a hoop layer is added in the subsequent step.

This is followed by the iterative loop, starting with the calculation of the Puck criterion. If the existing layup cannot compensate for the loads that occur, the critical point in the tank contour is determined. If this point is in the cylindrical tank segment, a hoop layer is placed and the next iteration loop is started.

In case the critical contour coordinate is in the conical tank segment or in the dome area, the winding angle is incremented within the defined constraints and the Puck criterion is applied for each increment. Based on the best optimization of the failure criterion, a layer with the associated orientation is added. This iteration continues until the reserve factors are satisfied and the optimized layup can be concluded.

3.2.3 Post-processing

In post-processing, the data determined in the simulation are output and can be used as a basis for subsequent evaluations. These data sets can be summarized under the following categories.

- **Masses:** Depending on the geometry, the number of layers and their orientation, the final tank mass is obtained. This mass is composed of the partial masses of the tank shell itself, the liner mass, the mass of the insulation, and the mass of the fairing.
- **Design:** Resulting from the optimized lay-up design given, the number of layers and its orientations are exported after the simulation of the winding process. In addition to determining the overlap of the wound strips, the output data also includes material-specific characteristic values, such as the exact fiber mass resulting from the percentage distribution of the fiber and matrix.
- **Computation:** In addition to the tank parameters, simulation specific values such as simulation time and number of iterations can be extracted.

3.3 Evaluation

The final evaluation is based on the comparison of different tank geometries defined by the TLRs of conceptualized hydrogen aircraft. In order to realistically consider the resulting requirements, an existing aircraft geometry is used as the basis for the evaluation. This fuselage geometry defines the design space available for the integration of the tank, which in turn is limited to the rear fuselage section of the aircraft in the context of this evaluation.

Due to the conical shape of the aft fuselage area, this results in two extreme tank geometries, a purely cylindrical shape and a conical shape constrained by the aft restriction of the design space. Through an iterative adjusting of the geometric parameters, tank shapes that lie between these extreme positions can be obtained. A subsequent regression of the simulation results

allows a complete representation of the tank geometries that can be realized in the design space. These simulation results are basically evaluated based on two different criteria groups.

3.3.1 Criteria tank design

Some of the comparison parameters derived from the simulation results are related to the tank itself and neglect aspects related to the overall aircraft design. These are further explained in the following paragraphs.

Geometry

The parameterization of the conical tank section, the cylindrical length resulting from the volume requirements and the dome contours yield the absolute length of the tank. From this and the tank diameter, among other things, the influence of the overall dimension of the tank can be derived.

Layup and masses

Various data can be drawn from the layer structure of the respective tank configurations, which also allow in-depth material evaluation. For the evaluation within the scope of this work, the focus is placed on the resulting total empty tank mass, which consists of four submasses explained below:

- **Shell mass:** The shell mass is considered as the mass of the wound composite material. Its mass can be therefore taken from the post-processing of the simulation.
- **Insulation mass:** The insulation is assumed to have a constant thickness around the tank with defined geometrical and material properties. Respecting the thickness of the wound tank, the total mass is computed using these geometrical properties.
- **Liner mass:** The tank geometry determined by the geometric parameterization corresponds to the outer contour of the liner. The shape is therefore independent of the number and orientation of the layers and its mass can be computed with the assumption of a constant wall thickness and the density of the liner material.
- **Fairing mass:** The fairing is an additional 0.5 mm thick cover made of kevlar attached to the insulation to protect the foam-based system from external influencing factors.

Surface-to-volume ratio

The surface-to-volume ratio is defined as the ratio of the tank surface and its storage volume. On the basis of this characteristic value, a basic assessment of the thermal properties of the tank can be made, since the heat flux has a linear dependence on the surface area [23].

$$\text{Surface-to-volume ratio} = \frac{\text{Tank surface}}{\text{Tank volume}} \tag{3.5}$$

An in-depth thermal analysis requires the determination of the thermal parameters of the tank and therefore shows the need for further extensive design decisions, which include the design of the integration structure among others. Therefore, this parameter serves only as an initial assessment and can be used subsequently for a more comprehensive thermal evaluation.

Gravimetric index

The gravimetric index gives the ratio of the mass of the stored fuel and the overall mass including the empty tank, installation, system and fuel mass. Thus, this parameter indicates the percentage of the stored fuel in relation to the overall mass.

$$\text{Gravimetric ratio} = \frac{\text{Fuel mass}}{\text{Total mass}} \tag{3.6}$$

Aiming to minimize this ratio, the impact of different configurations on the overall tank mass can be compared and an optimized structural design can be concluded. Depending on the definition of this parameter, the mass of the related systems such as the fuel pumps and valves are included in the system mass. Since this investigation is focused on the tank itself and the determination of the system and installation mass requires further design steps in order to obtain its total mass, the mass assumptions are taken from the overall aircraft design.

3.3.2 Criteria Overall Aircraft Design

Contrary to the evaluation based on the parameters defined in the chapter 3.3.1, this analysis refers to the global impact of the tank on the overall aircraft design. The mass rating is based on two different partial masses, the total tank mass and the fuselage mass.

As defined above, the tank mass is the sum of the shell, insulation, liner and the fairing mass and the mass of the related systems. In order to maintain a constant fuselage length for passengers and payload, certain tank configurations require an extension of the cylindrical fuselage section to allow the integration of the tank. The resulting mass of the elongated fuselage is approximated based on comparable fuselage sections of existing aircraft configurations and is evaluated in relation to the tank configuration. Summing these two masses up, the resulting total mass of each configuration is obtained and can be used as a basis for the overall aircraft design as an initial mass estimation.

3.4 Surrogate model

Since the simulations are time-consuming and depend on the application, a surrogate model can be created, on the basis of which the final simulation results can be approximated. This enables an assessment of the tank parameters, such as mass and surface, as a function of the geometric parameters, particularly in the preliminary design, and can thus narrow down the design space of interest before the simulations are carried out.

In order to define the design space covered by the surrogate model, a design of experiments is performed. To carry out this, the upper and lower boundaries of each design variable needs

to be set. By specifying the number of grid points, a uniform grid is obtained, which results in a two-dimensional mesh when two parameters are considered.

Based on this grid, simulations are performed in the following step, which takes into account the variation of all parameters in the increments defined by the number of samples. To do this, the simulation parameters are varied so that each increment of each parameter is included once in the tank configuration.

In order to derive a continuous function from the discrete simulation results, a regression is performed using the kriging method. This method determines the function value at a given point by computing a weighted average of the adjacent known values. This allows a reliable approximation of the function to the undetermined points and thus allows an assessment of the variation in results depending on the geometric parameters.

Finally, a graphical representation can be used to show the dependence of the simulation variables on the geometric properties. Due to the multidimensional dependence, a representation of all parameters in a single graph is not possible.

Chapter 4

Simulation

4.1 Design

The central design decisions often represent a compromise between the various optimal solutions of the different subsystems. In addition, there are certification requirements that map the framework conditions of the design and whose compliance represents the highest prioritization in the development process. These are explained in more detail in the following section.

4.1.1 Certification aspects

The minimum requirements necessary to certify an aircraft of the size studied here are set forth in CS25. The criteria defined there for the design of the tank are described in more detail below.

In addition to the design according to the structural loads occurring during flight operations, tanks must also take into account the hydrostatic loads of the stored fuel. These can be determined by the equation defined in section CS25.963 (d) (1).

$$P = K\rho gL \tag{4.1}$$

with P being the hydrostatic pressure, K the load factor, ρ the fuel density, g the acceleration due to gravity and L the length of the liquid column.

Due to the integration of the tank within the fuselage structure, the load factor in forward direction is 9, in upward and lateral direction 3 and 6 in downward direction. Respecting the load direction, L corresponds either to the tank diameter (for upward, downward and lateral) or the tank length (for forward and backward).

Another aspect included in the certification is the definition of safety factors. Due to the technological novelty of hydrogen-powered aircraft, the tank-specific requirements are defined in a separate special condition with reference to the storage of hydrogen in the aircraft environment. This states that in order to achieve the limit load of the inner tank, a safety factor of 1.33 to the operating range must be taken into account in the structural design. Under this load case, permanent detrimental deformation resulting in leakage and a safety limitation must be prevented.

To reach the ultimate load, a further safety factor of 1.5 is multiplied to the previously determined limit load. The tank structure must be subjected to this load for at least 3 seconds before the structure is allowed to fail or leak resulting in hazardous conditions. This definition allows the interpretation that only a safety factor of 1.33 needs to be considered in the design of the tank with inter fiber failure but under the condition that the liner of the tank prevents fuel leakage and after applying the additional safety factor to reach the ultimate load, no fiber failure occurs within the prescribed time period [26].

Another requirement under CS25.953 is the independence of the fuel systems that supply the engines. In the specification considered here, this requirement results in the need for two separate tank systems whose independent functionality must be ensured. According to this definition, no common insulation may be used between the tanks, which in turn affects the positioning of the tanks.

4.1.2 Pressurization

The tank pressure represents a compromise from a structural, aircraft design, and systems engineering standpoint. From a structural point of view, the aim is to minimize the pressure difference in order to decrease the resulting loads and thus reduce the number of plies required and its mass. At the same time, however, a lower maximum internal tank pressure leads to a higher fuel loss due to venting due to the lower difference from the minimum tank pressure, and thus the fuel mass required for the flight mission is higher. This in turn results in a higher structural mass caused by the bigger dimensions of the tank.

The fuel supply systems attached to the tank system, on the other hand, require a higher operating pressure in order to ensure, depending on the type of system, that the engines are supplied by the pressure differential. Alternative architectures supply the drive unit with fuel via a pump system, which requires lower tank pressure, but results in additional mass with high-maintenance components. Based on these facts and by evaluating various analyses in the literature, the maximum operating pressure was set at 2 bar.

Regardless of these design considerations, the internal tank pressure must be above the ambient pressure at all times during operation to prevent ambient air from entering the tank and causing a reactive hydrogen-oxygen mixture. The maximum ambient pressure during operation is 1 bar at ground level, resulting in a minimum operating pressure of 1.1 bar.

4.2 Geometry

The geometrical dimensions mainly depend on the required fuel volume which in turn results from the defined flight mission and the constrains given by the fuselage architecture. These factors are further detailed in the following chapters.

4.2.1 Design space

In order to determine the tank geometries considered for the simulation, the design space must be defined in a preliminary analysis. For the application studied in the context of this thesis, the fuselage architecture of a DLR aircraft concept is used.

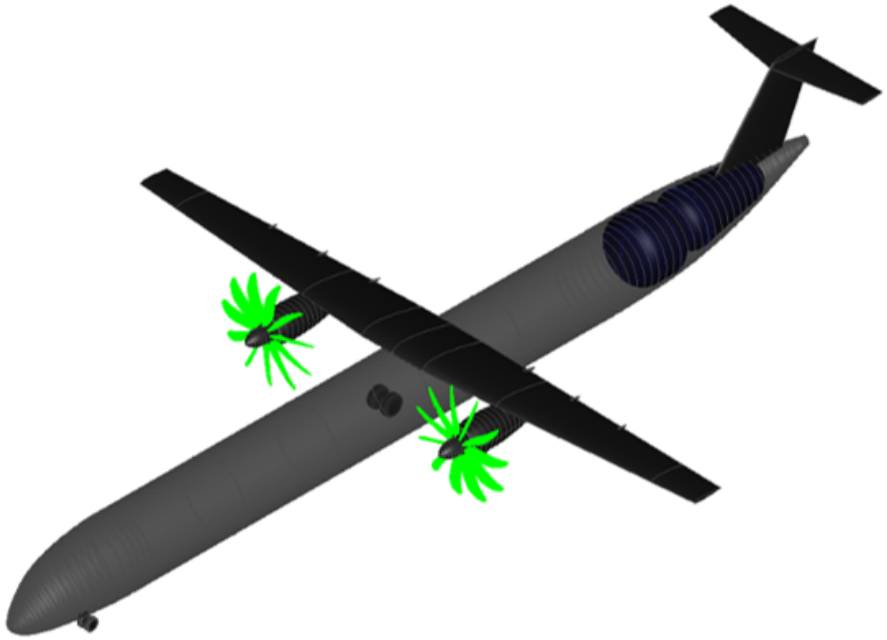

Fig. 4.1. Reference aircraft D250-TPLH2-2040

This aircraft concept is designed for a maximum passenger capacity of 250 passengers with a range of 1500 NM. The propulsion are two turboprop engines that run on gaseous hydrogen which is stored in liquid form in cryogenic tanks in the rear section of the fuselage. The T-tail configuration allows a greater flexibility in tank geometry, which is why this aircraft concept is preferred for this study.

From the fuselage diameter, which varies along the longitudinal position, the maximum internal tank diameter can be derived based on the dimensions of the various components (Table 4.1) between the fuselage skin and the tank liner.

Table 4.1: Dimensions of components

Component	**Value [m]**
Fuselage outer diameter	3.950
Fuselage skin	0.003
Stiffening elements (frames and stringers)	0.100
Insulation	0.127
Tank skin	0.020
Tank inner diameter	3.450

Based on the contour line of the fuselage, while maintaining the minimum distance of 250 mm between it and the tank liner normal to the outer contour, the upper and lower contour of

the limits of the design space are defined. It is assumed that the cross-section of the fuselage is circular, regardless of the longitudinal position.

The rear boundary is defined by the constraints resulting from the position of the tail plane and the subsystems positioned in the rear of the aircraft. Due to the internal structural connection of the fuselage and the tethered subsystems as the APU, assuming that this configuration does not change with a new type of propulsion, the design space is set up to a position giving enough flexibility to install the structural connection and the mentioned subsystems. In the front of the design space no constraint is fixed to allow the adaptability of the length of the cylindrical sub-segment, which is given by the required tank volume. Combining these constraints, the defined design space is obtained (Figure 4.2).

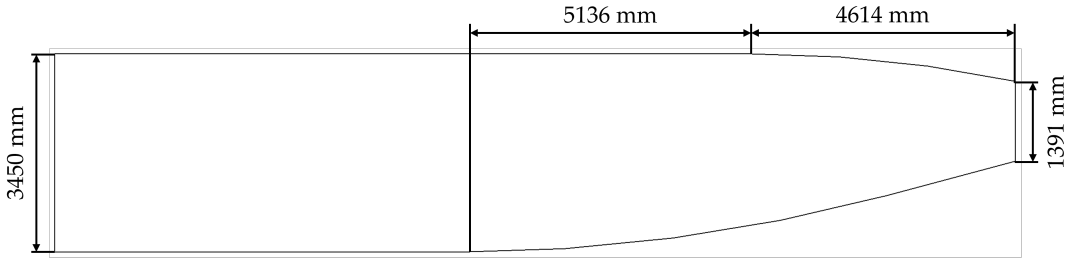

Fig. 4.2. Defined designspace

4.2.2 Dome type

Decisive for the dimensioning of the tank and the space-efficient integration in the aircraft environment is the dome contour. In order to objectively compare the dome contours explained in Chapter 2.4, the characteristics of two different tank shapes with alternating dome types are compared with each other.

The first configuration is a purely conical tank with a geometric parameterization corresponding to the rear fuselage section of the aircraft structure under consideration. The remaining geometric quantities, such as the maximum diameter as well as the length, are determined by automatic scaling of the tank to meet the volumetric requirements.

The second configuration is a cylindrical tank with the same volume requirements as the conical tank. Due to the alternating dome shapes, the cylindrical length of the tank is automatically calculated in accordance with the given volume requirement. The parameters of both tank shapes are given in table 4.2.

Table 4.2: Input parameters of tank configurations

Tank type	**V [m³]**	**POR [mm]**	**P [bar]**	**Alpha**	**Beta**	**Gamma**	**Cyl. d [mm]**
Conical	23.252	50	2	0.3	1	0.1	-
Cylindrical	23.252	50	2	-	-	-	3450

The evaluation of the different dome types is performed by comparing the geometric characteristics and the total masses of the tank, taking into account the liner, the insulation as well as the fairing masses.

The geometric evaluation of the conical tank is based on the longitudinal and radial dimensions. From this, the possible positioning of the tank in the fuselage can be derived given a defined design space. A small maximum diameter and axial length allows an integration further in the back of the fuselage. Due to the already predefined diameter in the cylindrical tank configuration, only the axial dimension is considered in the evaluation of this tank shape.

Due to the dependence on a second geometric parameter, the ratio of the semi-axes, different configurations of the elliptical dome are analyzed to cover the whole design range of this dome type. This ratio is varied in a range from 0.2 to 0.8 in increments of 0.2. The values determined are shown in Table 4.3 with the semi-axis ratio of the elliptical domes in brackets.

Table 4.3: Mass, diameter and length of tanks with alternating dome types

Tank	**Dome type**	**Total mass [kg]**	**Diameter [mm]**	**Length [mm]**
Conical	Hemispherical	477	2898	5354
	Elliptical [0.8]	469	2966	5033
	Elliptical [0.6]	490	3042	4685
	Elliptical [0.4]	503	3130	4317
	Elliptical [0.2]	679	3234	3926
	Isotensoid	415	3022	4634
	Torispherical	461	3170	4330
Cylindrical	Hemispherical	467	3450	3636
	Elliptical [0.8]	469	3450	3406
	Elliptical [0.6]	528	3450	3176
	Elliptical [0.4]	570	3450	2947
	Elliptical [0.2]	609	3450	2717
	Isotensoid	309	3450	3047
	Torispherical	538	3450	2954

To ensure that the magnitude of the respective comparison arguments does not influence the subsequent evaluation, the absolute values of mass, diameter and axial length are normalized. The value 0 corresponds to the lowest absolute value and the value 1 to the highest absolute value.

In order to take into account the importance of the three different properties in the evaluation, weighting factors are defined. These are subsequently multiplied with the normalized properties of the tank. The weighting of the tank mass accounts for 40 % of the overall assessment, while the geometric properties account for a total of 60 %. The higher proportion of tank dimensions is due to the fact that the larger tank geometry indirectly results in an increase in mass due to the required lengthening of the fuselage, and this has a high influence on the overall aircraft mass. For the conical tanks, the geometric evaluation parameter is divided in half between the diameter and the axial length of the tank.

These three values are then cumulated to obtain the overall rating, the minimum of which in turn represents the preferred dome type form for this application. The results are shown in Table 4.3.

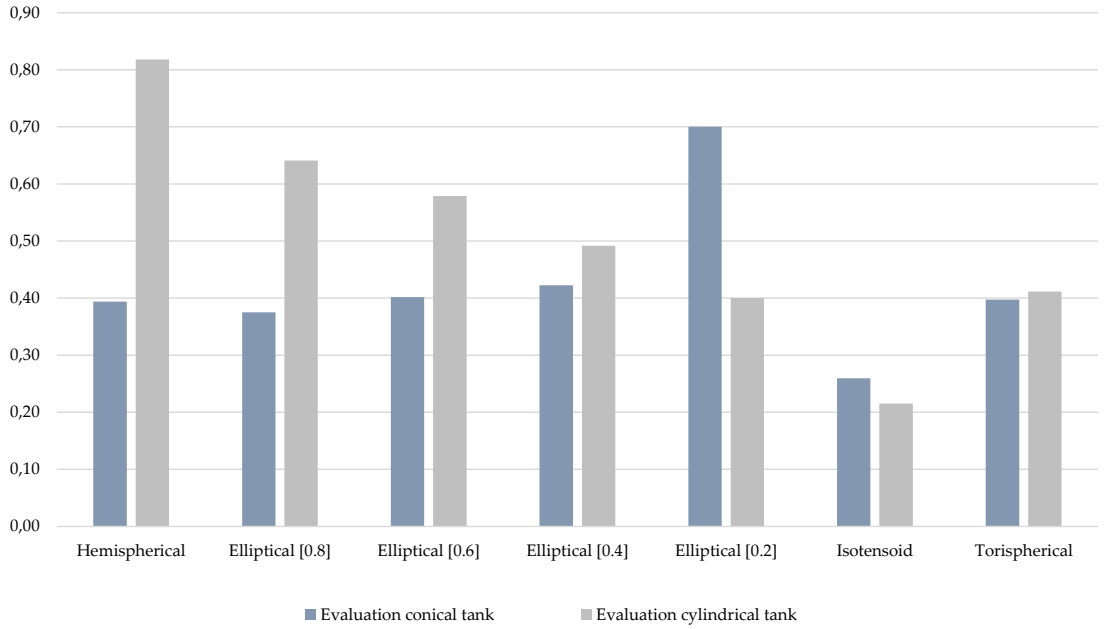

Fig. 4.3. Evaluation of dome types

It can be concluded that for a conical tank shape, the isotensoid dome is the best compromise. Despite the average tank diameter and axial length, the isotensoid dome has a significantly lower mass than the other dome types in comparison. The hemispherical and elliptical domes with a semi-axis ratio of 0.8 also show advantages, especially due to the likewise low mass and the smaller maximum diameter, but resulting from the wider design the axial length is higher compared to the tank with isotensoid dome ends.

The result of the evaluation of the dome contours for cylindrical tanks shows a clear difference between the different dome types. Especially due to the low mass, the isotensoid dome shows the best properties despite the medium axial length. Although the elliptical dome shape with the semi-axis ratio of 0.2 has the highest mass in the entire comparison, this design relativizes the result of the evaluation due to the small axial length and thus shows the second best properties in the overall comparison.

Following these results, an isotensoid dome is chosen for both, conical tank and cylindrical tank shapes.

4.2.3 Tank contour

Based on the previously defined design space and the chosen dome types, the contour line of the tank can be determined. Due to the non-rotationally symmetric design space and the desired high volume efficiency, the tank is inclined depending on the longitudinal position in the fuselage.

Due to the complexity of the design space, the position of the tank is determined by a two-dimensional approximation and with the help of a CAD program. For this purpose, four points are defined for the conical tank configuration, which lie on the symmetrical contour line of the tank and on the upper and lower contours of the design space. Two points each correspond to the minimum radius and two to the maximum radius of the conical tank segment. Due

to the convexity of the airplane fuselage, the conical segment is designed to be linear (except for the transition radius required for tangent continuity) to avoid intersection with the defined boundary of the design space.

Depending on the desired position of the tank in the fuselage, the small tank diameter can be fixed and an iterative process can be used to determine the remaining geometric parameters. In this process, the dimensions of the initial geometry are entered into the simulation program and automatically scaled by the volume requirements so that all requirements are fulfilled.

Based on the final dimensions, the angle between the longitudinal axis of the fuselage and that of the tank can be obtained in the subsequent step and the required rotation derived from this, which optimizes the volumetric efficiency.

In order to be able to represent all possible tank positions in the design space, one tank configuration each is considered in the foremost and rearmost area of the design space corresponding to a purely cylindrical and a conical shape. To perform a final regression based on these data, three additional configurations are defined at regular intervals between these positions.

The previously explained requirements according to CS25 incorporates two separate tank systems, which also include the insulation of the tank. This results in a required minimum distance between the two tanks, which can be computed with the thickness of the insulation and an additional distance of 100 mm for the integration structure. Due to the two-dimensional approximation of the position and the slight rotation of the tank, geometric deviations result which are compensated by a factor of 1.1 multiplied with the distance obtained. The geometrical properties of the different configurations can be taken from the table below.

Table 4.4: Parameters of different tank configurations

Tank	**Volume [m³]**	**Rotation [°]**	**Alpha**	**Beta**	**Gamma**
1 Back	23.252	4.32	0.441	1.331	0.100
1 Front	23.252	2.32	0.025	0.309	0.100
2 Back	23.252	5.03	0.136	0.667	0.100
2 Front	23.252	1.27	0.013	0.268	0.100
3 Back	23.252	2.37	0.056	0.384	0.100
3 Front	23.252	0.00	0.000	0.000	0.000
4 Back	23.252	0.95	0.009	0.257	0.100
4 Front	23.252	0.00	0.000	0.000	0.000
5 Back	23.252	0.00	0.000	0.000	0.000
5Front	23.252	0.00	0.000	0.000	0.000

With the maximum diameter determined from the automatic scaling, the final contour of the tank can be defined in the subsequent step. The geometries of the five configurations, each with two different tanks, can be seen in Figure 4.4. Since the cylindrical tank shapes have symmetry to the vertical axis in addition to rotational symmetry, these geometries are represented only by the half contour line.

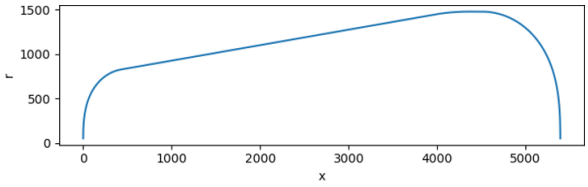

(a) Back tank of the first configuration

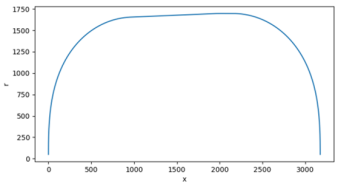

(b) Front tank of the first configuration

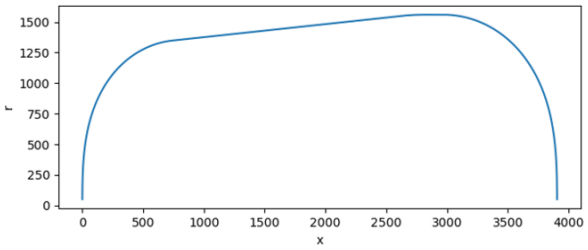

(c) Back tank of the second configuration

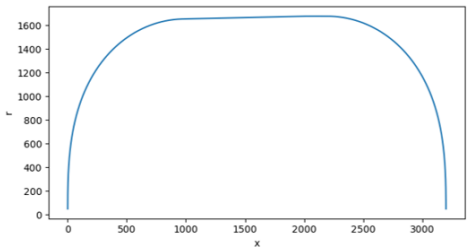

(d) Front tank of the second configuration

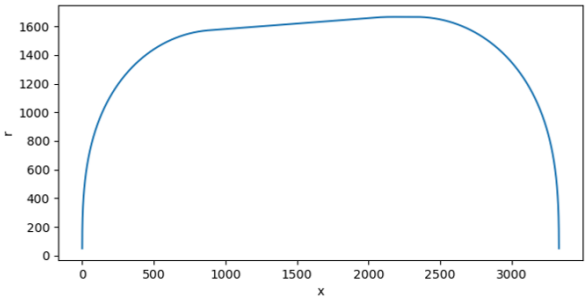

(e) Back tank of the third configuration

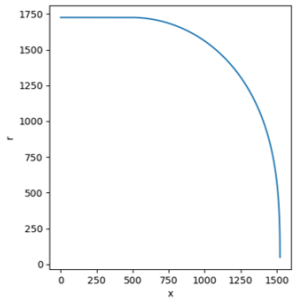

(f) Front tank of the third configuration

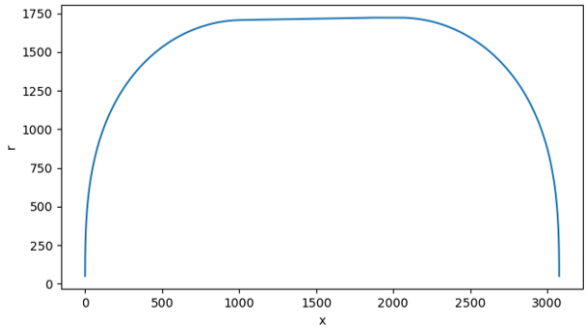

(g) Back tank of the fourth configuration

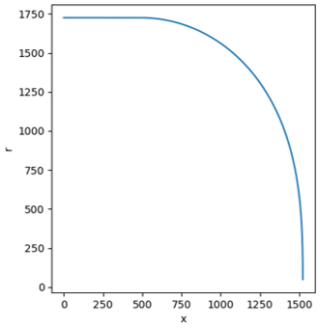

(h) Front tank of the fourth configuration

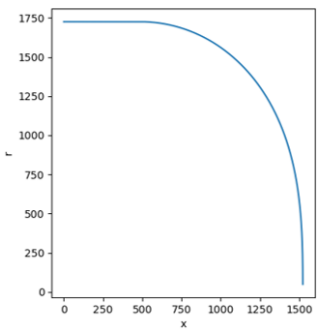

(i) Back tank of the fifth configuration

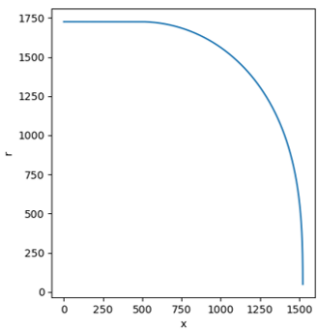

(j) Front tank of the fifth configuration

Fig. 4.4. Geometries of the different configurations

4.3 Manufacturing and material

The maximum orientation angle of a helix layer is set to 70° due to the given machine limits. The width of a single roving is set to 3.175 mm for the winding simulation. As a compromise of sufficient design flexibility and reduced production time, the number of parallel wound rovings is defined as 12, resulting in a bandwidth of 38.1 mm.

The material characteristics were taken from the default values of the simulation. These include in addition to the fiber and resin parameters also the fiber volume fraction, which is 0.62. Some basic properties of the material are shown in the table below with index 1 indicating the fiber direction and index 2 and 3 indicating the perpendicular directions.

Table 4.5: Material characteristics

Young's modulus [MPa]	**Shear modulus [MPa]**	**Poisson ratio**
$E_1 = 168640.5$	$G_{23} = 4012.0$	$\nu_{23} = 0.346$
$E_2 = 10800.0$	$G_{13} = 5140.0$	$\nu_{13} = 0.276$
$E_3 = 10800.0$	$G_{12} = 5140.0$	$\nu_{12} = 0.276$

4.4 Surrogate model

The first step in determining the surrogate model is to define the design parameters. For that, it is obligatory that they are independent of each other. This is true for the three geometric parameters α, β and γ. However, the volume and the maximum diameter show a dependence under certain conditions. This is given if the geometric definitions are not compatible with the volume requirement, so that the maximum tank diameter is scaled down. In this scenario, a dependency occurs that is undesirable for the investigation. To avoid this, instead of the volume, the cylindrical length of the tank section is defined. This shows no dependence on the other parameters, regardless of the tank configuration.

To cover the entire design range, the lower and upper boundaries of the respective parameters are set. Both parameters α and γ are valid by their definition in a range from 0 to 1. Even though the extrema 0 and 1 are mathematically defined for both of these parameters, they represent unrealizable tank shapes in practice. For example, the value 1 of α corresponds to a tank with a minimum radius of the conical tank section of 0 mm. In order to limit the parameterization to realistically representable tank contours, the lower and upper limits of these two parameters are therefore adjusted.

The lower limit of the cylindrical length corresponds to the minimum value required by the winding software. The upper limit, on the other hand, is set at a sufficiently high value of 4000 mm to be able to cover large-volume tanks.

To define the limits of the cylindrical diameter, existing aircraft fuselage architectures are consulted. The maximum fuselage diameter for a classic short-medium range aircraft is about 4 m, which allows a maximum tank diameter of 3.5 m, taking into account insulation and stiffening elements. The lower limit is set based on estimates where the minimum feasible cylindrical diameter is determined for conical tank shapes.

Respecting these constraints, the upper and lower boundaries for the design space are obtained and shown in Table 4.6.

Table 4.6: Lower and upper boundaries

	Alpha	**Beta**	**Gamma**	**Cylindrical length [mm]**	**Diameter [mm]**
Lower boundary	0.1	0.5	0.1	150	2000
Upper boundary	0.9	3.5	0.9	4000	3500

Since the number of samples is congruent with the number of simulations to be performed, and consequently the simulation time is linear to the number of samples, a compromise must be found between sufficient accuracy and the calculation time of the substitute model. Even with a theoretically considered infinite number of sampling points, a deviation occurs. Among other things, this is due to the discrete number of layers and the resulting mass jumps, which leads to a non-differentiable function.

As a compromise of these two aspects, the number of samples was set to 20. This results in increments of 0.04 for the α and γ parameters, 0.15 for the β, and 192.5 mm increments for the cylindrical length and 75 mm for the cylindrical diameter.

Chapter 5

Results and evaluation

5.1 Tank evaluation

Based on the previously defined simulation parameters and the five configurations with two tanks each the results are evaluated. Following the methodology described in chapter 3.3, the tank itself is evaluated in the first part.

5.1.1 Tank geometry

From the contour of the conical tank section defined by the parameterization, the cylindrical section is scaled according to the volume requirements. With the dome ends of the tank, the total length is obtained without taking insulation and fairings into account.

To assess the effects of the tank position on its length, the position of the tank center, as well as its front and rear end positions, are plotted in normalized design space and arranged according to the location of the center as shown in Figure 5.1.

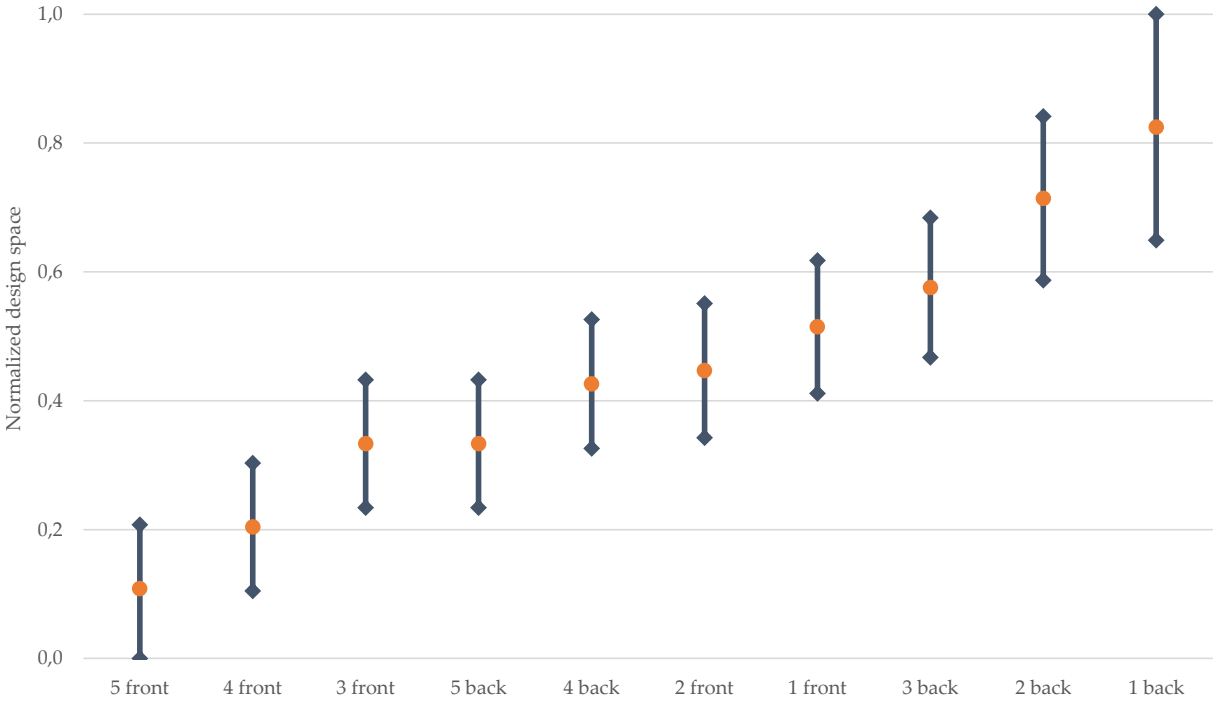

Fig. 5.1. Tank length

In this graphic, the orange dot represents the position of the tank center. The diamond-shaped blue dots indicate the ends of the tank on both sides while the length of the line corresponds to the normalized tank length. The geometries of the front tanks of the third, fourth and fifth configurations and the rear tank of the fifth configuration correspond to cylindrical shapes, which is why only the position and not the length of the tanks differ.

In the different shapes, it can be seen that the penalty due to conicity has very little effect on the overall length of the tank. Only the rear tanks of the first and second configuration show significant differences in length.

5.1.2 Design of layup

The orientation and number of layers is determined by the optimizer. The final design of the layups of the different tank configurations are tabulated below.

Table 5.1: Design of layups

Tank	**1** [°]	**2** [°]	**3** [°]	**4** [°]	**5** [°]	**6** [°]	**7** [°]	**8** [°]	**9** [°]	**10** [°]
1 back	2.7	70.0	34.4	47.8	9.9	44.7	57.0	40.2	70.0	10.5
1 front	2.3	70.0	9.8	70.0	70.0	9.8	69.5	-	-	-
2 back	2.5	70.0	59.9	10.0	62.1	67.5	10.3	68.6	-	-
2 front	2.4	70.0	10.1	69.8	69.9	69.5	10.1	-	-	-
3 back	2.4	69.9	10.0	69.9	69.4	69.6	10.1	-	-	-
3 front	2.3	90.0	9.7	90.0	90.0	9.9	90.0	-	-	-
4 back	2.3	70.0	9.4	69.7	69.7	8.9	70.0	-	-	-
4 front	2.3	90.0	9.7	90.0	90.0	9.9	90.0	-	-	-
5 back	2.3	90.0	9.7	90.0	90.0	9.9	90.0	-	-	-
5 front	2.3	90.0	9.7	90.0	90.0	9.9	90.0	-	-	-

The number of layers, except for the rear tanks of the first and second configurations, has no dependence on the geometry of the tank. Both the cylindrical and conical shapes have a total of seven layers. In addition, the percentage distributions of the layer orientations of the conical tanks also show no dependence on the tank shape with a small variation of the conicity. With a percentage of 57 %, the conical tank geometries with low conicity (the front tanks of the first and second configurations and the rear tanks of the third and fourth configurations) have a high percentage of plies with an orientation of approximately 70°. The remaining plies (excluding the initial helical layer with the angle defined by the tank shape and pole opening radius) are at an angle of about 10°. Only the order of the last two layers varies in these configurations. The two remaining conical tank shapes have a higher number of plies, eight and ten, respectively, and have in addition a higher variation of ply orientations.

The majority of the layers of the cylindrical tank shape are hoop layers with a share of 57%. The second and sixth layers have orientations around 10°, similar to the geometries with a low conicity.

5.1.3 Tank masses

From the defined tank geometries the masses of the sub-components such as the shell, liner, insulation and fairing mass are obtained in the post-processing of the simulation. These masses can be taken from the table below.

Table 5.2: Masses of sub-components

Tank	Surface	Shell [kg]	Liner [kg]	Insulation [kg]	Fairing [kg]	Total [kg]
1 back	66	203	31	198	34	466
1 front	50	114	26	168	29	337
2 back	57	140	28	177	30	375
2 front	40	113	27	168	29	337
3 back	51	122	27	169	29	347
3 front	40	88	26	167	29	310
4 back	49	113	26	167	29	335
4 front	40	88	26	167	29	310
5 back	40	88	26	167	29	310
5 front	40	88	26	167	29	310

It can be seen from the data that the variation in liner mass is small, with a difference of 5 kg between the minimum and maximum corresponding to a percentage of 19 %. The mass of the fairing shows a similar order of magnitude. Here, too, the difference between the various tank geometries is small at 17 %. Due to the small proportion of the total mass of the tank, this variation can be neglected.

In contrast to these two partial masses, the mass of the insulation (apart from the rear tank of the first configuration) accounts for most of the total weight. However, the values here also differ to a small extent at approximately 18 %.

The differences between the masses of the various configurations, despite the same tank volume, can be explained by the different surfaces of the tank. The geometry of the rear tank of the first configuration has the highest conicity of the shapes studied. According to the mathematical definition, a cone has a higher surface area than a cylindrical body for a constant volume. As the shapes of the tank get closer and closer to a cylinder, the surface area decreases and so do the masses of the insulation and fairing mounted outside the tank, respectively the liner located on the inside.

The shell mass, in contrast to the other partial masses, shows higher differences. The maximum difference is 115 kg between the rear tank of the first configuration and the cylindrical shape, a percentage difference of 130 %. This difference may be due to two aspects, among others. One of these, as with the partial masses mentioned previously, is the higher surface area of the first tank. Due to this, a higher quantity of material is required per layer to ensure complete coverage.

The second aspect is related to the number and orientation of the layers. With 10 layers, the rear tank of the first configuration has the highest number compared to the other tank geometries. In addition, a majority of these layers have low to moderate orientation angles.

This also results in a higher amount of material per layer, which in turn leads to a higher mass. The cylindrical tank shape, on the other hand, has 57 % of hoop layers, which, due to their positioning in the cylindrical area, require a smaller quantity of material than helical layers and therefore also have a lower mass.

The sum of these four partial masses gives the total mass of the tank considered here. To show the relationship between the positioning of the tank in the design space and its mass, the normalized location of the tank center is used. Based on this data, the relationship shown in Figure 5.2 below is obtained.

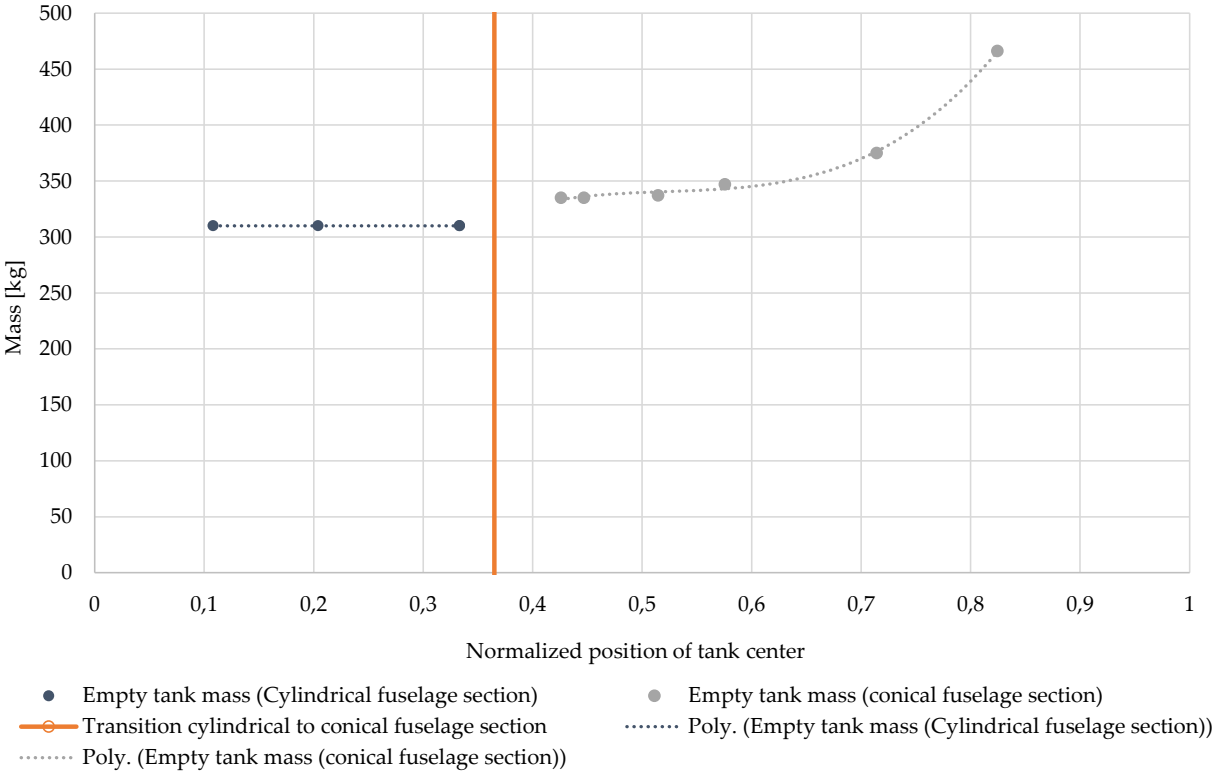

Fig. 5.2. Normalized tank position against tank mass

In the low range of the normalized position of the tank, the masses have a constant value. This can be explained by the fact that the tanks are positioned in the cylindrical part of the design space and the geometry is thus congruent. At the position of 0.36, the transition from the cylindrical to the conical fuselage area is located, which results in a jump of the masses. This is partly due to the fact that no circumferential layers are placed in these configurations and the lower orientation angles result in higher masses per layer.

In the range from approximately 0.42 to 0.52 the mass behaves almost constant. This can be justified by the fact that the conicity of the design space in this region changes only slightly with increasing longitudinal coordinate. As a result, the variation of the tank shapes in this area is small, which means that the influence on the total mass is also low. This justification is congruent with explanation resulting from the layer structure. Even if the order of the layers differs in these three tanks, the total number and the number of layers with the respective orientations are almost identical and, as a result, this mass is also identical.

As the longitudinal coordinate increases from a normalized position of 0.57, the mass increases exponentially. This is primarily due to the also increasing conicity of the design space and the tank shape, which have a higher number of layers than the previous configurations.

5.1.4 Surface-to-volume ratio and gravimetric index

For further comparison and evaluation of the different tank configurations, the parameters explained in more detail in Chapter 3.3 are used. These are shown graphically in the figure below.

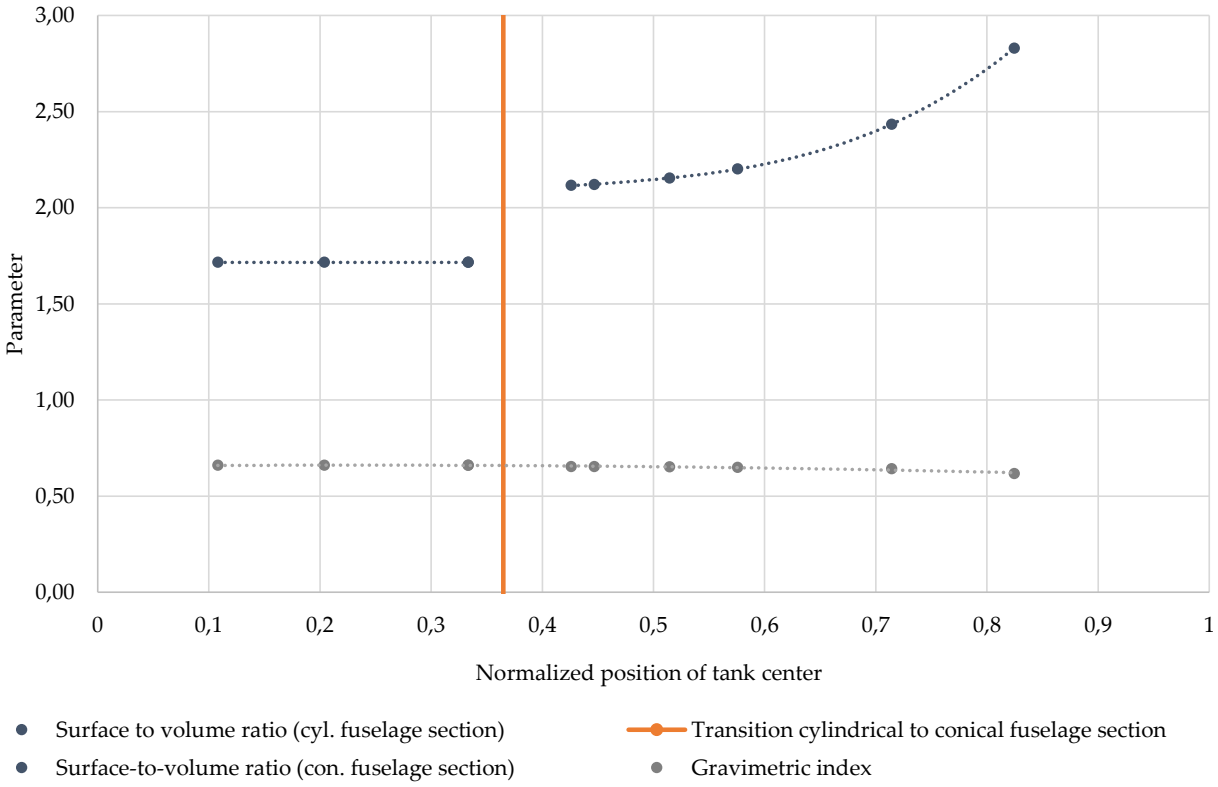

Fig. 5.3. Normalized tank position against evaluation criteria

As in the previously performed analysis, the tank shapes with a higher conicity have a larger surface area. Due to the constant volume of the configurations considered here, the surface-to-volume ratio increases with increasing longitudinal position. Due to the abrupt increase in surface area when crossing the boundary between the cylindrical and conical design space, there is also a significant increase in the parameter from approximately 1.7 to 2.1. With increasing longitudinal position, this characteristic value also shows an exponential course with a maximum of 2.83.

Due to the linear relationship between surface area and heat flux, this configuration exhibits the greatest thermal heat flux, resulting in an increased boil-off rate. However, this relationship can only be evaluated qualitatively in this comparison and requires a more extensive thermal investigation.

The gravimetric index, on the other hand, shows a nearly constant behavior over the entire design space. This is primarily due to the low percentage of the structural mass on the total

mass of the tank system. Since not only the structural but the total mass of the associated systems, the installation structure and the stored fuel are added to determine the index, the mass of the tank itself corresponds to a share of only 24 to 29 %. The individual masses used for this calculation were taken from the overall aircraft design with 338 kg for the system mass per tank, 114 kg for the installation mass per tank and 1482 kg for the mass of the stored hydrogen per tank.

The variation of the gravimetric index of only 6 % reflects a dependence between the position of the tank but for the tanks with a low conicity this can be neglected, since these values differ only by one-hundredth. The small proportion of the structural tank mass in the total mass also has the effect that, unlike the other comparative variables, there is no sudden increase at the transition from the cylindrical to the conical section of the design space.

5.2 Overall evaluation

The integration of the tanks and associated systems influence the overall aircraft design through their architecture and characteristics. This primarily includes the position of the tank in the aircraft fuselage. For the analysis carried out as part of this work, the position of the tank was restricted to the rear fuselage area. This results in necessary adjustments to the fuselage length in order to integrate the tank while maintaining a constant passenger capacity.

Since both tanks of the respective configuration are required for the fulfillment of the flight mission, this global comparison does not consider the individual tanks but the entire configurations. For this purpose, the average position of both tanks is used and the total mass is determined as the sum of both individual tanks.

To determine the additional mass due to the fuselage extension, the mass of the fuselage per unit length must be determined on the one hand, and the required cylindrical length depending on the configuration on the other. For mass determination, data from the aircraft design of a comparable concept with the same type of propulsion as well as wing configuration are used as the reference aircraft of this study.

The mass of the empty fuselage is 14310 kg with a length of 51.7 m. For further calculation, the average mass per meter is used, which in this case is 277 kg/m. Even though it can be assumed that the mass is not homogeneously distributed over the entire length of the fuselage, the accuracy of this value is sufficient to obtain an approximation of the additional mass.

The calculation of the additional fuselage length is done using the CAD data of the tank positions. The tank section positioned in the cylindrical design space results in an extension of the fuselage and is therefore congruent with the additional fuselage length. For the fifth configuration, the length of both tanks is assumed due to the position, minus the dome length of the rear tank, since this can be integrated into the conical section due to its curvature.

These data are summarized with the resulting total mass in Figure 5.4.

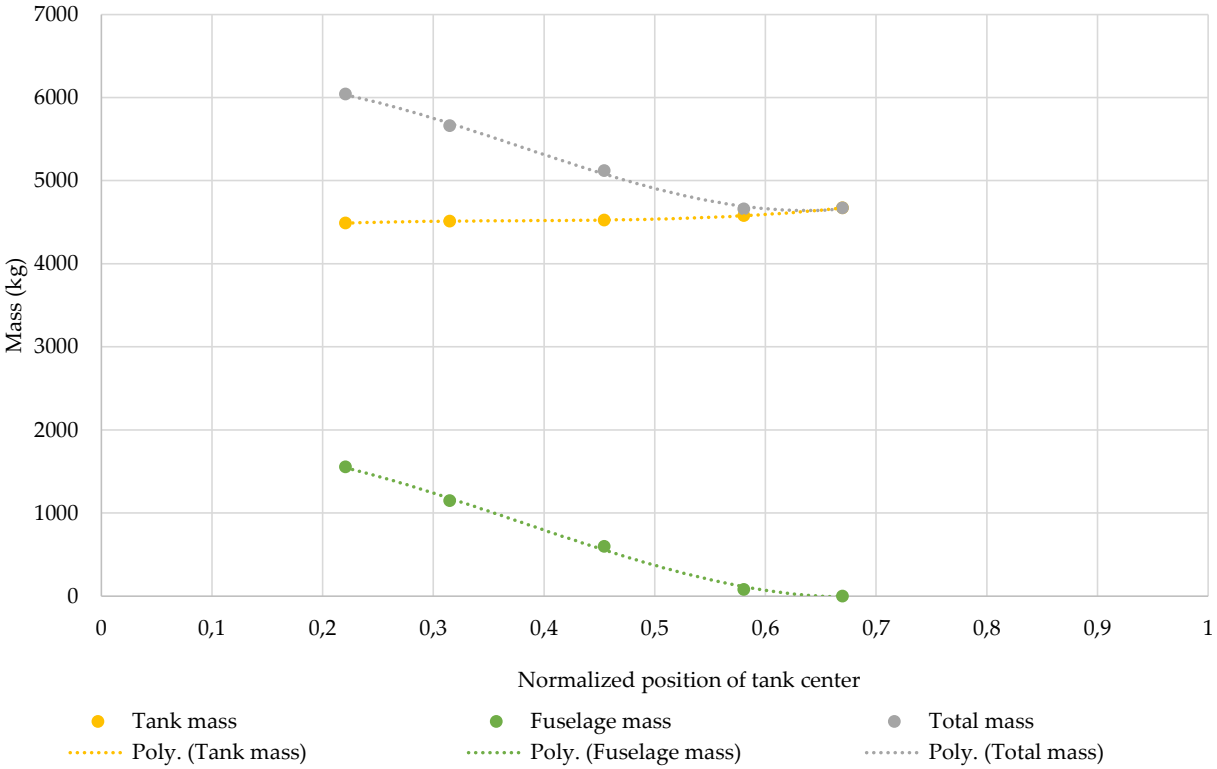

Fig. 5.4. Normalized tank position against total masses

The tank mass shown in this plot is composed of the structural mass derived from post-processing of the simulation and the masses of the hydrogen, the systems, and the integration structure.

The resulting mass of the fuselage shows an almost linear progression with a maximum of about 1500 kg belonging to the first configuration. Due to the integration of both tanks of the this configuration in the conical section, an extension of the fuselage is not necessary.

The total mass, which results from the addition of the tank mass and the fuselage mass, shows a similar trend as the graph of the fuselage mass due to the almost constant tank mass in percentage terms. Due to the opposite course of the graph of the tank mass, the graph of the total mass converges. This is due to the fact that the mass resulting from the fuselage extension is compensated by the lower mass of the tank. As a result, the first and second configurations show an almost identical total mass.

5.3 Surrogate model

Due to the multidimensional dependence of the simulation results, a representation of all parameters in three-dimensional space is not possible. To relate to the previously performed assessment, the total mass of the tank and its surface area are represented in the surrogate model. In order to improve the display of the variation of the results in dependence of the individual parameters, they are graphically shown separately from each other. The unmapped parameters are each held constant at the mean value of the respective lower and upper bounds.

The variation of the parameters and their influence on the total mass of the tank, which is composed of the shell, liner, insulation and fairing mass, are shown in the figures below.

The mass shows a negative linear dependence on the parameter alpha. The small variation of the mass over the entire parameter space is to be emphasized here. With only approximately 5 %, this is considerably lower compared to the parameter beta, the cylindrical length and the diameter.

The course of the β mass graph shows an almost positive linear behavior. As the β value increases, the total mass of the tank also increases. Compared to the α parameter, however, the difference between the minimum and maximum mass in the design space shows a much higher change with a factor of approximately 3. This is mainly due to the large geometric changes in the longitudinal axis of the tank caused by the change in this parameter.

The parameter γ shows a linear increase comparable to the previous graph. However, it should be pointed out that the variance of the mass over the entire design space is only 0.5 kg, which corresponds to 0.01 % in percentage terms. Therefore the mass is considered as constant. Over the entire parameter space, however, the volume increases by about 10 %.

The relationship between the length of the cylindrical tank section and the total mass of the tank also shows a linear progression. The linearity can be explained by the fact that due to the extension of the cylindrical section, the load case does not change, but the additional mass results from the necessary covering of the tank surface. This leads to significant mass increases, which amount to approximately 80 % in the entire parameter space.

In contrast to the other graphs, the graph of the cylindrical diameter does not show a linear but an quadratic course. This can be explained, among other things, by the fact that the surface of the domes, if they are approximated as hemispherical geometries, increases quadratically with the radius. If the number and orientations of the layers are not taken into account, this results in a non-linear increase in mass.

In order to be able to evaluate the inaccuracy of the model and thus also to assess the significance, the maximum deviation of the regression function from the actual value of the simulation can be determined.

For this purpose, the differences from existing simulation results with the function values of the regression are formed and the parameters of this configuration are output.

The highest deviation occurs in the configuration at the parametric values of $\alpha = 0.77$, $\beta = 0.75$, $\gamma = 0.53$ and the cylindrical length of 964 mm and the cylindrical diameter of 3250 mm with a square mean of 58 kg, which corresponds to a percentage difference of approximately 10 %. Since this represents the maximum occurring deviation of the model, it can be stated that the deviation of the model in the entire parameter space is at most 10 %.

Comparable to the above illustration of the effects of tank geometry on tank mass, the relationship to surface area can also be illustrated. These can be seen in the diagrams below.

The correlations of the parameters and the surface of the tank mainly show similar linear behavior as the previously shown connections between the tank mass and the parameters. Small deviations are shown by the graphs of the parameter and the cylindrical diameter. Similar to

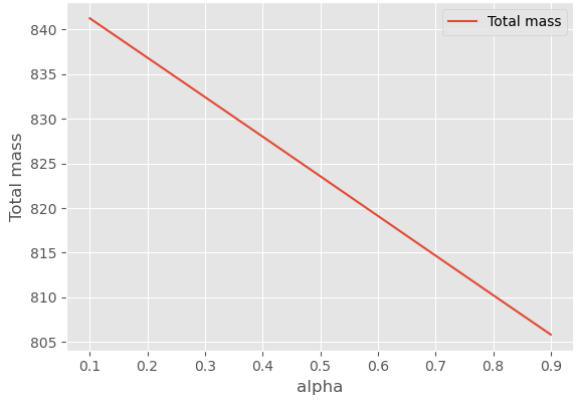

(a) Parameter α against total tank mass

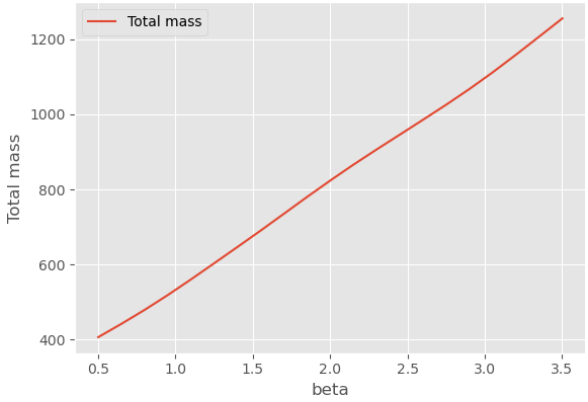

(b) Parameter β against total tank mass

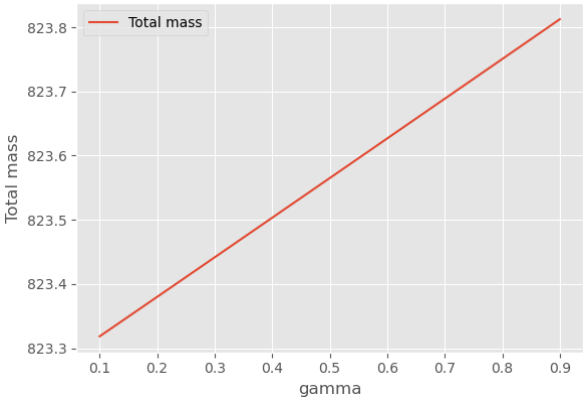

(c) Parameter γ against total tank mass

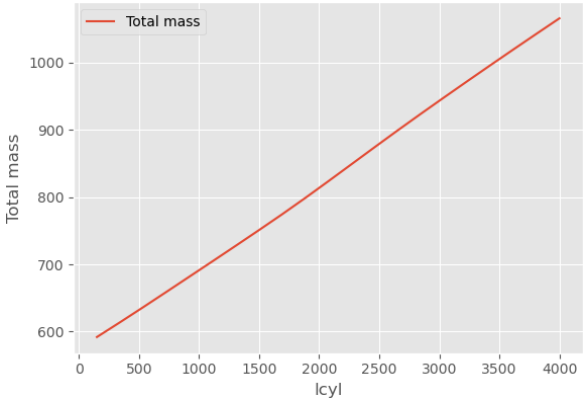

(d) Cylindrical length against total tank mass

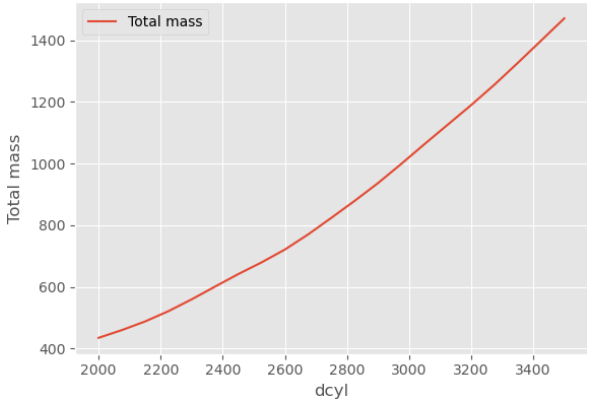

(e) Cylindrical diameter against total tank mass

Fig. 5.5. Impact of geometrical parameters on tank mass

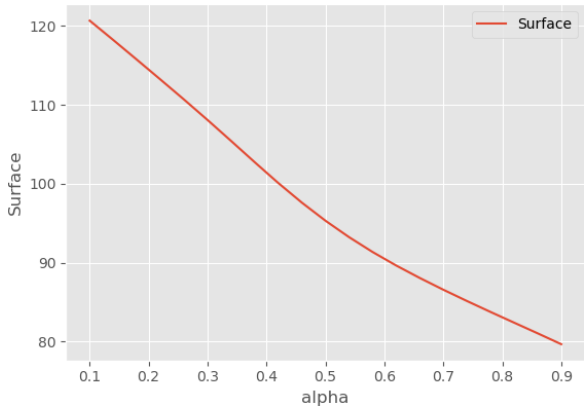

(a) Parameter α against surface

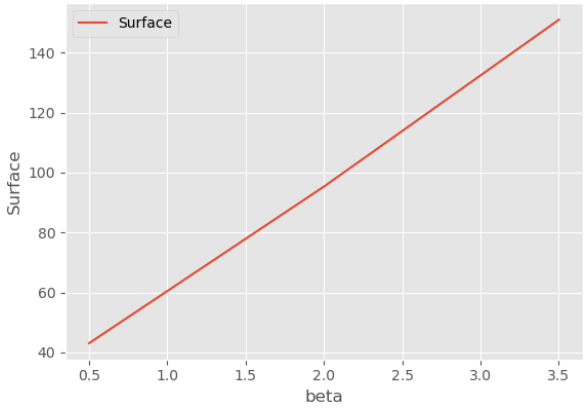

(b) Parameter β against surface

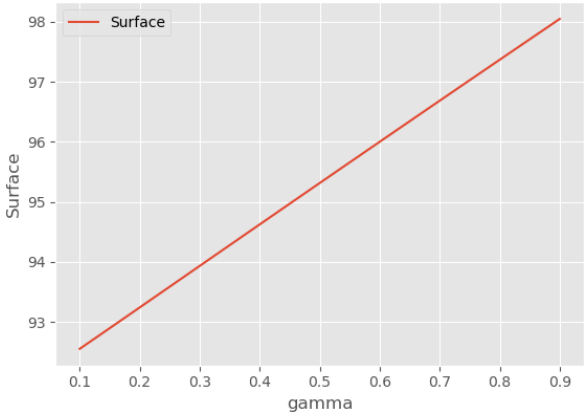

(c) Parameter γ against surface

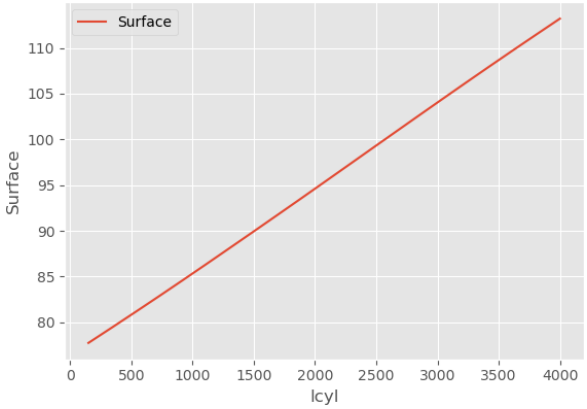

(d) Cylindrical length against surface

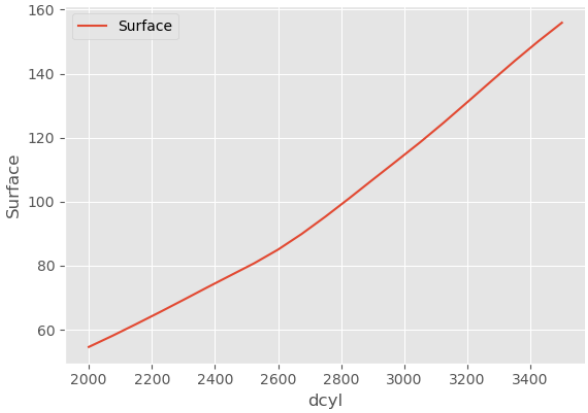

(e) Cylindrical diameter against surface

Fig. 5.6. Impact of geometrical parameters on tank surface

the relationship to the mass, this can be attributed to the quadratic increase in the area of the dome. This behavior can be seen in the graph of the parameter alpha, since this represents the ratio of the cylindrical and minimum conical diameter. If the value of alpha tends towards 1, the conical diameter tends towards 0, which results in a reduction of the surface area. However, since the quadratic relationship only applies to the dome sections of the tank, this behavior is only evident to a small extent in the sum of the individual subareas.

However, clear differences can be seen in the magnitude of the variations. While, similar to the mass, the parameter gamma shows only small differences of the surface in the entire parameter space, the other parameters show clearer differences such as β and the cylindrical diameter. Both of these show a difference of a factor of 3.75 and 3.2 respectively. Again, this can be attributed to the large influence of these two parameters on the overall tank shape.

For evaluation, the maximum deviation of the function from the real value can also be determined by the quadratic mean for this model. For this model, the maximum difference is 8.15 m², which is given by the parameters $\alpha = 0.5$, $\beta = 1.25$, $\gamma = 0.84$, as well as the cylindrical length of 3384 mm and a diameter of 3500 mm. In percentage terms, this corresponds to a deviation of approximately 7 % measured against the actual surface of this configuration.

Chapter 6

Conclusion and outlook

6.1 Conclusion

Based on the results of this work, meaningful conclusions can be drawn for future projects.

From the comparison and evaluation of the individual tank configurations, it is clear that cylindrical geometries offer the best properties. Irrespective of the evaluation criterion, this tank shape shows clear advantages over the conical shapes. These include first and foremost the structural mass, which is up to 50 % lower. The properties resulting from the smaller tank surface also offer advantages, especially with regard to the thermal behavior of the tank.

However, if the effects on the overall aircraft design are taken into account, these tank shapes exhibit contrary behavior. The necessary lengthening of the fuselage results in a significant increase in the aircraft's mass. The superposition of the masses leads to an almost equal mass of the two most conical configurations in the aircraft concept considered here. Therefore, neglecting other factors such as influence on the handling, a recommendation can be made for these tank shapes.

In addition, the architecture of the aircraft fuselage is critical to the design of the tank. In order to be able to integrate large-volume tanks in a space-efficient manner, a fuselage section with low conicity has advantages, as this allows the length of the tank to be reduced while maintaining a constant volume. However, since the shape of the conical fuselage section also affects the aerodynamics of the entire aircraft, a compromise must be found here to optimize the overall performance of the aircraft.

Furthermore, the position of the tail also plays a role in the dimensions of the available design space. Novel tail arrangements can thus allow greater freedom of tank integration.

Another finding is that it makes sense to precisely match the tank shape to the fuselage contour using the gamma parameter, as this has almost no effect on the tank mass, but can lead to an increase in volume of up to 10 %.

Both the fuselage elongation and the positioning of the tank have an influence on the flight behavior of the aircraft due to the changed center of gravity. Especially the very far back center of gravity of the tank has a considerable influence on the handling due to the changing mass during the flight mission.

6.2 Outlook

With the integration of conical tank shapes into the winding simulation, there is greater flexibility in the geometric design. In the future, this can also be used for the preliminary design of new aircraft through the developed parameterization. For this purpose, a detailed comparison of metal and CFRP tanks can be used to determine the effects on the tank's characteristics and to identify application-specific solutions.

The findings of this work can also be used to focus on other topics. One of these is the exact evaluation of the influence of the tank extension and the tank position on the flight characteristics. Both aspects have a negative effect on the center of gravity due to the increased mass in the rear fuselage area. Based on this, an analysis of the effects on wing position and tailplane dimensions can be carried out.

Another aspect is the detailed design of the tank insulation. The size of the surface area, which depends on the tank shape, influences the thermal behavior of the tank and thus requires a specific insulation system. An analysis can therefore include a detailed dimensioning of the insulation depending on the tank shape and the resulting mass penalty. In addition, other insulation methods can be considered and evaluated from a thermal point of view.

Another project may look at comparing metal and CFRP tanks. Both materials offer advantages for specific applications and have differences in manufacturing processes and costs. Metal tanks can offer advantages in this area, and it is also possible to draw on empirical values from the aerospace industry but CFRP shows advantages in the design capability and usually has a lower mass compared to metal tanks.

In addition, the manufacturing methods of CFRP tanks can be discussed in more detail. Although wound tanks offer structural advantages, the introduction of local reinforcements is not possible. This aspect is of great importance for the design process, especially with regard to integration and the resulting point loads. Possibilities would exist in the unification of winding and taping processes in order to combine the respective advantages of both methods.

Bibliography

[1] National Oceanic and Atmospheric Administration. *Climate Change: Global Temperature*. 2021. URL: https://www.climate.gov/news-features/understanding-climate/climate-change-global-temperature (visited on 05/12/2022).

[2] International Energy Agency. *Global CO2 emissions from transport by subsector, 2000-2030*. 2021. URL: https://www.iea.org/reports/tracking-transport-2021 (visited on 05/13/2022).

[3] International Energy Agency. *Global Energy Review: CO2 Emissions in 2020*. 2021. URL: https://www.iea.org/articles/global-energy-review-co2-emissions-in-2020 (visited on 05/12/2022).

[4] D. Silberhorn et al. "Climate Impact Reduction Potentials of Synthetic Kerosene and Green Hydrogen Powered Mid-Range Aircraft Concepts". In: *MDPI* (2022).

[5] United Nations. "Paris Agreement". In: (2015).

[6] Airbus. "Airbus Global Market Forecast 2021 - 2040". In: (2021).

[7] G. D. Brewer. "Hydrogen Aircraft Technology". In: *CRC Press* (1991).

[8] P. Agarwal et al. "Injector Design Space Exploration for an Ultra-Low NOx Hydrogen Micromix Combustion System". In: *Proceedings of ASME Turbo Expo 2019* (2019).

[9] A. Gomez and H. Smith. "Liquid hydrogen fuel tanks for commercial aviation: Structural sizing and stress analysis". In: *Aerospace Science and Technology* (2019).

[10] Flake C. Campbell. "Structural Composite Materials". In: ASM International, 2010, p. 141.

[11] A. Brent Strong and Catherine A. Ploskonka. "Fundamentals of Composites Manufacturing". In: Society of Manufacturing Engineers, Publications Development Department, Reference Publications Division, 1989, p. 120.

[12] L. Zu. "Design and optimization of filament wound composite pressure vessels". 2012.

[13] S. T. Peters, W. D. Humphrey, and R. F. Foral. "Filament Winding Composite Structure Fabrication". In: *ASM International* (1991).

[14] Ö. Özbek. "Determination of mechanical behaviors of filament wound hybrid composite pipes". 2019.

[15] Suong V. Hoa. *Principles of the Manufacturing of Composite Materials*. Department of Mechanical, Industrial and Aerospace Engineering, 2017.

[16] Y. Su et al. "Review of the Hydrogen Permeability of the Liner Material of Type IV On-Board Hydrogen Storage Tank". In: *World Electric Vehilce Journal* (2021).

[17] A. Kayran and C. S. İbrahimoğlu. "Preliminary study on the applicability of semi-geodesic winding in the design and manufacturing of composite towers". In: *Department of Aerospace Engineering, Middle East Technical University* (2012).

[18] P. Bose et al. "A survey of geodesic paths on 3D surfaces". In: *Computational Geometry: Theory and Applications* (2011).

[19] T. Sofi, S. Neunkirchen, and R. Schledjewski. "Path calculation, technology and opportunities in dry fiber winding: a review". In: *Advanced Manufacturing: Polymer and Composites Science* (2018).

[20] L. Zu, J. Wang, and S. Li. "Integrated design and production of filament-wound composite structures: compromise between strength and manufacturability". In: *20th International Conference on Composite Materials* (2015).

[21] F. C. Shen. "A filament-wound structure technology overview". In: *Materials Chemistry and Physics* (1995).

[22] S. Koussios. "Filament Winding: a Unified Approach". 2004.

[23] S. K. Mital and J. Z. Gyekenyesi. "Review of Current State of the Art and Key Design Issues With Potential Solutions for Liquid Hydrogen Cryogenic Storage Tank Structures for Aircraft Applications". In: *NASA* (2006).

[24] L. Zu, S. Koussios, and A. Beukers. "Application of isotensoid-based cross sections to filament-wound toroidal pressure vessels". In: *Design and Production of Composite Structures* (2009).

[25] J. C. Murphy. "Filament-wound isotensoid pressure vessels having geodesic domes". In: *European Patent Application* (1996).

[26] EASA. "Appendix A - Special condition - Fuel cell and liquid hydrogen storage system". In: ().